PHYSICAL REVIEW B VOLUME 47, NUMBER 16 15 APRIL 1993-II

Growth and structure of Fe and Co thin films on Cu(111), Cu(100), and Cu(110): A comprehensive study of metastable film growth

M. T. Kief and W. F. Egelhoff, Jr.
Surface and Microanalysis Science Division, National Institute of Standards and Technology, Gaithersburg, Maryland 20899
(Received 2 November 1992)

The growth and structure of Fe and Co thin films on single-crystal Cu(111), Cu(100), and Cu(110) substrates have been investigated using x-ray-photoelectron and Auger electron forward scattering, CO-titration, low-energy electron diffraction, and reflection high-energy electron diffraction. The motivation for this study is to understand the role of surface structure and kinetics in the growth of metal films on metal substrates. The effect of varying substrate growth temperatures between 80 and 450 K plays a prominent role in determining both the film morphology and crystalline phase. Nonideal film growth, including agglomeration of Co and Fe and surface segregation of Cu, is the rule rather than the exception. Simple considerations of surface diffusion and surface free-energy differences provide a basis for understanding why layer-by-layer growth is unlikely to occur in these systems and should not be expected in many other metastable film-substrate systems.

I. INTRODUCTION

Substantial research has sought to understand the diverse structural and magnetic properties of thin films of Fe and Co grown on Cu. These systems are employed in the research fields of surface magnetism, low-dimensional magnetism, magneto-optics, giant magnetoresistance, and many others (see Ref. 1 and references therein). The applications of this research span from magnetic recording media and recording heads to nonvolatile memory chips. Unfortunately, the results of these research studies have often been contradictory. This confusion is largely due to an inadequate understanding of the film growth, film morphology, and the delicate interplay between thin-film structure and magnetic properties. Therefore, it is timely to examine the building blocks of these structures namely, monolayer films of Fe and Co epitaxially grown on Cu(111), Cu(100), and Cu(110).

We report the structure and morphology of Fe and Co films prepared by molecular-beam epitaxy on single-crystal Cu substrates. We interpret these results in terms of the film-growth dynamics. To examine the effects of substrate structure, the film-growth mode has been studied on Cu(100), Cu(100), and Cu(111) with varying substrate preparations. To explore the effects of varying growth kinetics upon the system structure, films were grown at substrate temperatures ranging from 80 to 450 K. Presented here is a systematic and comprehensive structural study of these metastable systems using several complementary techniques including x-ray-photoelectron and Auger electron forward scattering, low-energy electron diffraction (LEED), reflection high-energy electron diffraction (RHEED) and CO titration.

Epitaxial growth of a metal film on a metal substrate is often categorized according to three standard models: two-dimensional or Frank–van der Merwe (FM) growth, three-dimensional or Volmer-Weber (VW) growth, and two-dimensional followed by three-dimensional or Stranski-Krastanov (SK) growth. According to the quasiequilibrium description by Bauer,[2] these three growth modes are governed by the surface free energies, the interface free energy, and the strain energy. The deposited film will grow in two dimensions or layer-by-layer (FM) if

$$\sigma_f - \sigma_s + \sigma_i + \sigma_e < 0 \ , \tag{1}$$

where σ_f is the deposited film surface free energy, σ_s is the substrate surface free energy, σ_i is the interface surface free energy, and σ_e is the strain energy. Otherwise, the film nucleates as three-dimensional clusters (VW). In the event that the inequality reverses with film thickness, layer-by-layer growth is followed by three-dimensional growth (SK).

A common goal in epitaxy is to produce two-dimensional film structures with a particular crystallographic phase and orientation. To attain this goal, we often desire FM growth. However, FM growth is difficult to obtain for Fe/Cu and Co/Cu because the surface free energies[3] of Co (2.709 $\mathrm{J\,m^{-2}}$) and Fe (2.939 $\mathrm{J\,m^{-2}}$) are significantly larger than the surface free energy of Cu (1.934 $\mathrm{J\,m^{-2}}$). In addition, since the heats of mixing for both Fe-Cu and Co-Cu are endothermic,[4] we can expect the interface free energies costs to be unfavorable. According to Eq. (1), the initial equilibrium growth of Fe and Co on Cu should be similar to VW, not FM as has been frequently reported.[5–24]

Furthermore, the quasiequilibrium VW growth mode predicted by Eq. (1) is frequently not obtained. Nonequilibrium growth can occur because kinetic factors (such as surface diffusion) are too slow. The actual film growth can result in departures from equilibrium structures and crystallographic changes [e.g., Fe/Cu(111)]. In addition, the three idealized growth modes neglect the possibility that substrate atoms can be mobile and may segregate to the surface during film growth. The importance of surface segregation is exemplified by its

widespread prediction and observation in metallic alloys.[4,25–27]

To understand whether equilibrium growth can be expected, we must identify the controlling processes. Three important processes relevant to metal-film on metal-substrate growth are (i) surface adatom diffusion, (ii) substrate surface segregation, and (iii) film/substrate interdiffusion. These processes are activated by increasing the substrate temperature during film growth. For a process to be significant, its rate should be compared to the film deposition rate, which is typically around 1 monolayer/min. In addition, it is essential to recognize that surface diffusion varies with crystal face and surface quality as well as element.

Activation energy barriers for surface diffusion have been measured for some metal/metal systems.[28–48] Typically, the measured surface diffusion barrier ranges from near 0.1 to 0.9 eV for different metals and different crystal faces. The surface diffusion process is assumed to follow an Arrhenius diffusion law, $D_0\exp(-E_d/k_BT)$, where E_d is the activation energy, k_B is the Boltzmann constant, T is the temperature, and with a typical preexponential D_0 of $\sim 10^{-3}$ cm^2/s.[28,29,32] Activation energies of 0.1–0.9 eV translate to about 40–350 K for an adatom mobility of 1 hop/s. As an example of the crystal face dependence, Ir self-diffusion has been determined to have activation energies of 0.27 eV for Ir/Ir(111),[30] 0.7 eV for Ir/Ir(110),[48] and 0.84 eV for Ir/Ir(100).[31]

The experimentally determined activation energy for self-diffusion on Cu(100), has been reported to be 0.28±0.06 (Ref. 49), 0.39±0.06 (Ref. 50), and ~0.48 eV.[51] Since other experimental surface diffusion data for Cu data are not available, we must rely solely upon theoretical estimates for self-diffusion on Cu(111) and Cu(110). Recent effective-medium calculations predict diffusion barriers for Cu(111), Cu(110), and Cu(100) of 0.13, 0.18, and 0.21 eV, respectively.[52,53] Since surface diffusion barrier energies are not available for many materials, it is useful to have a simple means to approximate them. An estimate of the diffusion barrier can be obtained by scaling the activation energy of an unknown material to a known material using the cohesive energies. Using the cohesive energy ratio for Cu/Ir=0.502 (Ref. 54) gives activation energies of 0.14, 0.35, and 0.42 eV for Cu on Cu (111), Cu(110), and Cu(100), respectively. The Cu(100) estimate agrees reasonably with the experimental values. However, the theoretically calculated Cu(100) value of Hansen *et al.*[52] is roughly half the experimental values.[55]

Segregation of the substrate atoms may occur when the substrate surface free energy is lower than the deposited film surface free energy. It is difficult to estimate the activation energy for this process, since in addition to surface free-energy differences, heats of solution and the elastic size mismatch energy may also play a role.[4] Furthermore, there may be more than one contributing segregation path (see Ref. 56 and references therein). However, we can expect that segregation may be important for Fe and Co on Cu for growth temperatures near and above room temperature because of experimental reports of significant segregation near 400 K for Fe and Co on Cu(100).[16,57–59]

Finally, the upper temperature limit for layer-by-layer equilibrium growth is imposed by requiring an abrupt film/substrate interface. Assuming that interdiffusion occurs through bulk diffusion and with a typical growth time of ~100 s, a growth temperature upper limit is estimated to be near ~0.5 the melting temperature. The upper limit for Cu, Co, and Fe is about 675, 885, and 900 K, respectively. Growth of films at temperatures above this threshold can often produce interdiffused or alloyed layers, even for systems that satisfy Eq. (1).

The limits imposed by these mobilities, combined with the film deposition rate, create a temperature window where equilibrium FM growth may occur.[60,61] For systems, such as Fe/Cu and Co/Cu, which do not satisfy the Eq. (1) criteria for FM growth, layer-by-layer growth may not exist at all. Therefore, in systems of high-surface free-energy metals deposited on low-surface free-energy substrates, we have chosen an alternate approach: deposit the film at low temperature where thermal diffusion is minimal, then anneal the system to a temperature that improves the lattice ordering but does not permit substrate segregation. This technique produces very-high-quality films.[62] Nevertheless, the emphasis of the present study is upon examination of the growth process and characterization of the as-grown film/substrate system. Careful annealing of a film grown at low temperature should be considered an additional, valuable tool to optimize the film quality.

In summary, it is essential to consider the growth kinetics in these metastable thin-film systems. Simple considerations of surface free energies and atomic mobilities provide a foundation for understanding the nonideal growth modes and structures of metastable Fe and Co films on Cu(111), Cu(100), and Cu(110). Furthermore, these ideas are expected to be equally valid and applicable to other thin-film systems.

This paper is organized in six sections. The Introduction (Sec. I) is followed by a review of the experimental methods (Sec. II). Growth on the different substrates is examined individually: Cu(111) (Sec. III), Cu(100) (Sec. IV), and Cu(110) (Sec. V). Within each of these three sections, film growth is discussed (A) in detail for Fe, (B) in detail for Co, and (C) in general for both Fe and Co with an emphasis on common aspects. A brief, general conclusion with specific highlights is given in Sec. VI.

II. EXPERIMENT

The molecular-beam epitaxy (MBE) system used in this work has two ultrahigh vacuum chambers. A long-stroke sample manipulator traverses the central axis of the chambers. The sample can be cooled to 80 K, heated to 1000 K, and rotated by a stepper motor about the main axis of translation. The first chamber contains the sputter ion gun, quadrapole mass spectrometer, LEED system, RHEED system, and metal MBE sources. The system base pressure is 8×10^{-9} Pa. A second adjacent chamber is equipped with a commercial x-ray source and a 150-mm mean-radius hemispherical electron-energy analyzer with input electron optics. The x-ray source and analyzer axis are 90° apart in the plane defined by rota-

tion of the sample normal. The x-ray photoelectron spectroscopy (XPS) and Auger data were obtained with Al $K\alpha$ (1486.6 eV) radiation. The analyzer has a 16-channel parallel detector for improved signal to noise. The geometric acceptance angle of the input electron-optics is $\pm 5°$, which was satisfactory for routine XPS and CO-titration measurements (described below). Improved angular resolution was desirable for forward-scattering measurements and was obtained by inserting an additional aperture, which reduces the acceptance angle to $\pm 2.5°$. The estimated absolute angular accuracy of these measurements is $\pm 1°$ with significantly better relative accuracy of $\pm 0.25°$. Further details of the MBE system are given in previously published work.[62]

All copper substrates were cut from a single-crystal boule using a wire-slurry saw. Each crystal was oriented to better than 0.5° with a diffractometer. The mechanically damaged layer was then removed from both sides of the substrate using an acid polishing instrument.[63] The crystal orientation was then rechecked with the diffractometer. A final, near-mirror finish was obtained by a brief, manual acid polish. The acid polishing solution[64] is formulated to produce optically flat metal surfaces and is based upon a solution of HCl acid, polyethylene glycol, and 2-mercaptobenzimidazole saturated with $CuCl_2$. The removal of much of the damaged layer at the crystal surface is demonstrated by the observation of a weak LEED pattern without any further cleaning or annealing. To remove impurities, the crystal was sputtered using Ar^+ or Ne^+ and annealed to ~ 900 K until no contamination was detectable with XPS and a sharp pattern was obtained with LEED.

All films were grown in a vacuum of 1×10^{-8} Pa or better. Fe was evaporated from a metal oven described elsewhere.[65] Cobalt was deposited from a tungsten-wire-filament evaporator. Typical film growth rates were ~ 2 monolayers/min as measured by an ion-gauge integration system.[62] Film thicknesses were measured by two quartz crystal monitors, symmetrically adjacent to the sample. The calibration of these monitors was done using RHEED oscillations. The average film thickness accuracy is ± 0.10 monolayers (ML) on Cu(100) and Cu(111) and ± 0.15 ML on Cu(110).

Films were routinely checked with XPS to monitor film purity. No attempts were made to correlate film-growth mode with XPS intensity or Auger kinks on account of the dubious nature of this practice for many metal/metal epitaxial systems.[66,67] LEED was used to investigate film structure and morphology.

The crystal structure of the film was investigated using x-ray photoelectron and Auger electron forward-scattering measurements. This technique has recently been used to study many metal-film/metal-substrate systems by several groups.[57,68–71] The primary advantage of this method is its elemental specificity combined with its real-space correspondence to near-neighbor bond direction through enhanced forward-scattering intensity. Strictly speaking, this interpretation of the electron forward scattering is accurate only for electron kinetic energies of several hundred eV or greater. At lower kinetic energies, the electron scattering may be dominated by multiple-scattering effects that distort and obscure simple interpretation. A consistency check is provided by comparing the XPS and Auger angular anisotropies for several different kinetic energies ≥ 0.5 keV: true bond directions will exhibit intensity enhancements independent of the kinetic energy. Therefore, it is generally straightforward to determine the crystal structure of the film from fast and simple XPS or Auger electron angular anisotropy measurements. For pertinent reviews on forward scattering as a diagnostic tool see Refs. 68, 69, and 72.

The crystal structure of the film can also be ascertained by a comparison of XPS and Auger angular anisotropies from deposited films with those observed from pure single crystals. This has the inherent advantage of including multiple-scattering and interference effects. Figure 1 shows polar XPS and Auger angular anisotropies for Cu single crystals with surfaces oriented along the (100), (110), and (111) directions. The XPS and Auger angular anisotropy is defined as the angular-dependent intensity divided by the maximum intensity in the angular scan. The similarity between the anisotropies at the four kinetic energies, Cu $2p_{3/2}$ (552.6 eV), Cu $L_3M_{45}M_{45}$ (916.6 eV), Cu $3s$ (1362.6 eV), and Cu $3p_{3/2}$ (1409.6 eV), for each Cu crystal provides an excellent demonstration of the

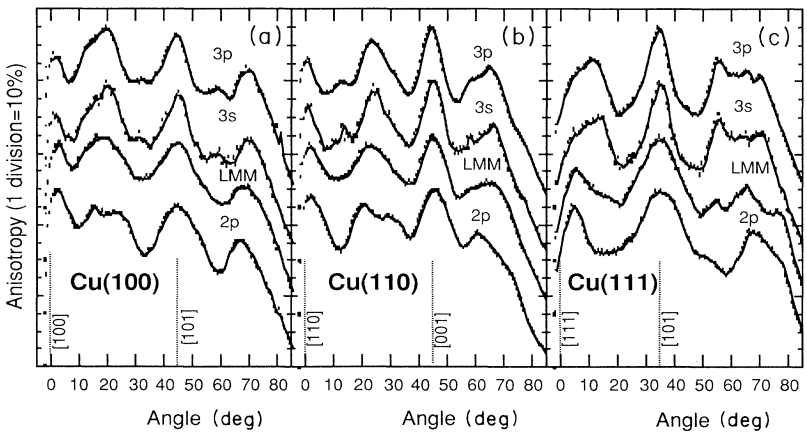

FIG. 1. XPS angular anisotropy vs polar angle for Cu(100), Cu(110), and Cu(111) in the ⟨001⟩, ⟨011⟩, and ⟨1$\bar{2}$1⟩ azimuths, respectively, using Al $K\alpha$ (1486.6 eV) radiation. Spectra are shown for four Cu x-ray and Auger energies: Cu $2p_{3/2}$ (552.6 eV), Cu $L_3M_{45}M_{45}$ (916.6 eV), Cu $3s$ (1362.6 eV), and Cu $3p_{3/2}$ (1409.6 eV). Nearest-neighbor directions are indicated by vertical dotted lines. Anisotropy is defined for each energy as (angular intensity)/(maximum peak intensity). The Cu(100) and Cu(110) 0° peaks appear asymmetric due to the grazing incidence of the Al $K\alpha$ radiation for this orientation.

forward-scattering phenomena. The indicated directions correspond to the crystal normal and to the strong forward-scattering directions that are associated with nearest- and next-nearest-neighbor axes. Scattering from more distant neighbors typically shows weak or no detectable enhancement unless it is compounded by first-order constructive interference effects.[69] A good example of this is the (100) crystal that has consistently strong forward-scattering peaks for all energies along [100] (0°) and [101] (45°) and additional features near 20° and 70°, which disperse slightly with energy. The 20° peak has been shown by simulations[73] to result from both a weak forward-scattering intensity along the [103] (18.4°) direction and a first-order interference maximum coincidentally near 20°, which disperses with electron kinetic energy. The peak near 70° also corresponds to a weak forward-scattering peak combined with a first-order maximum and is symmetric with the 20° maximum about the [101] direction. Similar interference maxima can also be observed in the other crystals, symmetric about the ⟨110⟩ directions.

Forward scattering serves to characterize the film crystallography, but does not provide direct elemental information about the surface layer. To answer difficult questions on film agglomeration and Cu surface segregation, a technique was developed to measure what fraction of the surface was exposed Cu or was "surface Cu." This procedure is referred to as CO titration and has been introduced previously.[62] The procedure is based upon the surface core-level shift of the Cu $2p_{3/2}$ state with adsorption of CO. Since only those Cu atoms exposed at the surface will have core-level shifts, the fraction of the surface that is Cu can be estimated by reference to a clean Cu substrate. To determine the amount of surface Cu for a particular sample, we deposit the film of Fe or Co and then measure the Cu $2p_{3/2}$ peak: (a) without CO, (b) with a saturation dose of CO at ~80 K, and (c) after warming to 300 K to desorb the CO from the Cu. The Cu $2p_{3/2}$ peak contains two contributions: (i) the signal from the surface Cu atoms, which shifts with CO adsorption, and (ii) the signal from nonsurface Cu atoms, which does not shift. To eliminate attenuation by the CO, the peaks are normalized to constant area, then the difference spectra (a)−(b) and (c)−(b) are calculated. (a)−(b) is called the *adsorption cycle* and (c)−(b) the *desorption cycle.* The resulting difference curves show a trough/peak shape that represents of the number of CO-shifted Cu surface atoms. The height of the difference curve for a given film is then compared to identical measurements on a clean Cu substrate with no film. The film/no-film height ratio corresponds to the fraction of the surface that is Cu. The adsorption cycle and desorption cycle estimates should be identical, within the estimated measurement uncertainty (±5%), if the number and kind of surface atoms remains constant after annealing to 300 K with adsorbed CO. Differences in the measurement cycles indicate undetermined instabilities, including film agglomeration and substrate segregation. We report both estimates to demonstrate the systematics of these measurements. However, when the adsorption and desorption measurements differ by more than the measurement uncertainty, we take the average as our best estimate of surface Cu and qualify these systems as metastable.

Generally, CO-titration measurements are made by measuring the Cu $2p_{3/2}$ intensity at a polar angle of 25°. For ideal flat films, measurements should show no change with detection angle in the fraction of the surface that is Cu surface. However, nonideal film growth can produce a variation with detection angle in estimated Cu. This is because measurements performed at 5° off the surface normal integrate contributions from all the Cu surface atoms equally, while measurements made near 80°, for example, will be less sensitive to Cu surface atoms at the bottom of cracks in the film. Therefore, additional angular-dependent CO-titration measurements were occasionally performed at 5°, 45°, 65°, and 80°. The variation in angle of the Cu estimate was then interpreted in terms of the distribution of the Cu surface atoms and the film morphology.

III. GROWTH OF Fe AND Co ON Cu(111)

The growth of Fe and Co on Cu(111) is a particularly rich system that has received considerable attention in the past. The structure of Fe films on Cu(111) has been studied using electron microscopy,[74–78] field-ion microscopy,[70] LEED, and Auger electron spectroscopy (AES).[10,80,81] The magnetic properties have been studied using torque magnetometry,[5–7,82] Mössbauer,[76] and electron-capture spectroscopy.[8] Similar structural studies of Co growth on Cu(111) have used LEED and AES,[18] and nuclear magnetic resonance (NMR),[83–87] surface-extended x-ray-absorption fine structure (SEXAFS),[88,89] x-ray scattering,[90] and XPS forward scattering.[91] The magnetic properties of Co/Cu(111) have been measured by torsion magnetometry,[92] ultraviolet photoelectron spectroscopy,[18,93] surface magneto-optic Kerr effect,[94,95] and torsion oscillation magnetometry.[96]

Table I shows that there is a very close lattice match to the Cu(111) surface net for both fcc and bcc phases of Fe, and both fcc and hcp phases of Co. In addition to the lattice match, the crystalline phase of the film is controlled by the epitaxial strain in the film. The equilibrium

TABLE I. Epitaxy of Fe and Co on Cu(111).

Material/ symmetry	Lattice constant (Å)	Nearest neighbor (Å)	Surface cell mismatch (%)	Interlayer spacing (Å)
fcc Cu(111)	3.61	2.55		2.08
fcc Fe(111)	3.59	2.54	−0.8	2.07
bcc Fe(110)	2.87	2.48	+3.4	2.03
fcc Co(111)	3.54	2.50	−3.9	2.05
hcp Co(0001)		2.51	−3.2	2.03

configuration of the strained film is predicted by minimizing the system free energy for all possible film crystalline phases, orientations, strains, and dislocations,[97,98] However, even this model of lattice mismatch and film elasticity is oversimplified, because it only considers continuous films. We will show below that there is no single epitaxial phase for Fe and Co on Cu(111). The epitaxial phase of the film depends on the growth temperature and the film thickness.

A. Fe/Cu(111)

Fe films were prepared at substrate growth temperatures of 80 and 300 K. The structure of these films was examined for thicknesses up to 8 ML. The fraction of Cu in the exposed surface was measured with both the adsorption and desorption CO-titration sequence as described above. These values were typically found to agree within 5%, which we believe is near our experimental accuracy. Therefore, we only report the average values. Figure 2 shows the fraction of Cu in the exposed surface versus film thickness. The fraction of Cu in the exposed surface increases with growth temperature and decreases with deposited Fe thickness. The data show that after deposition of about 3 ML of Fe grown at 80 K and 5 ML of Fe grown at 300 K the surface is 5% and 12% Cu, respectively. This agrees well with scanning tunneling microscopy (STM) estimates of 10% of the Cu substrate exposed for 4 ML of Fe deposited at 300 K.[99] Furthermore, annealing these films shows that they are stable. This thermal stability is demonstrated by the observations that a 2.3-ML grown at 80 K and a 5.6-ML film grown at 300 K show no increase in the fraction of Cu in the exposed surface for anneals of 300 K over the growth temperature. The large fraction of Cu at the surface indicates the Fe film growth is not an ideal layer-by-layer manner. This growth mode is in contrast to most of the literature,[5–10] which reports room-temperature FM growth of Fe/Cu(111).

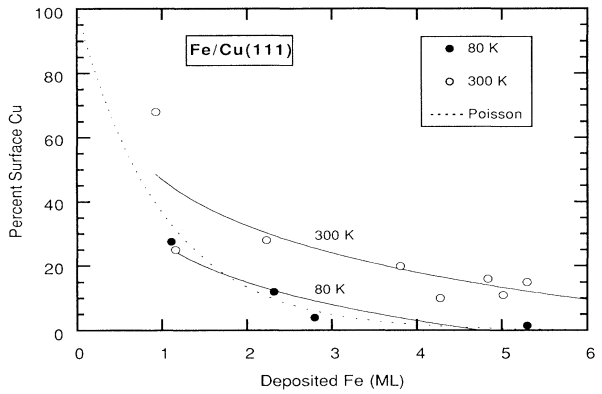

FIG. 2. The fraction of Cu in the surface for Fe deposited on Cu(111) at 80 and 300 K. Coverage is determined by the CO-titration technique using the average of adsorption and desorption measurements for 25° detection angle. Solid curves show an exponential fit to the drop in the measured fraction of Cu in the surface. The dotted line indicates the fraction of Cu in the surface for random substrate coverage according to Poisson statistics (see text for interpretation).

For comparison to the measured values, Fig. 2 shows the predicted values of the fraction of Cu in the exposed surface for the Poisson model. The Poisson model assumes random deposition on a simple cubic lattice. The direct comparison of the measured values with the Poisson model should be done with caution because the simple cubic lattice does not explicitly include the fcc(111) threefold adsorption geometry or stacking faults. If the adatoms have zero mobility, this model implies unphysical vacancies and overhangs. Relaxing this constraint and allowing the second layer adatoms to drop down into one of three possibly unfilled nearest-neighbor sites increases the substrate coverage to 52%, 21%, and 4% for depositions of 0.5, 1.0, and 2.0 ML, respectively. Comparing these new estimates with the simple cubic model prediction (Fig. 2) decreases the agreement, particularly for depositions above 1.5 ML. Alternatively, if the adatoms are somewhat mobile but cannot diffuse over a step and (or) the coverage is not random but locally correlated as occurs with small cluster nucleation, the simple cubic lattice Poisson estimate may be more appropriate. Examples of these types of growth are Pt/Pt(111) at 400 K (Refs. 100 and 101) and Fe, Co, and Cu on Cu(100) at 80 K.[102] Keeping these possibilities in mind, we have chosen always to plot the Poisson model estimates with the CO-titration measurements. The Poisson model estimate serves as a guideline for comparison between different materials, symmetries, and growth temperatures.

The crystalline structure of the Fe film was determined using forward scattering. Figure 3 plots the XPS angular anisotropies of Fe $3p_{3/2}$ (1431.6 eV) for films grown at 80 and 300 K and for depositions from about 1–7 ML.

The films deposited at low temperature, 80 K, show the evolution of a bcc Fe phase, which is indicated by a peak in the XPS angular anisotropy at 45°. The weak, broad rise near 45° with no 0° feature show the 1.0-ML film is nearly flat. The rise of a peak at 0° for a 2.3-ML film signifies the start of the third bcc layer, which is consistent with nearly layer-by-layer growth. Increasing the film thickness shows increasing structure in the angular anisotropies that indicate a bcc film.

A 1.0-ML film deposited at 80 K has a LEED pattern that is $p(1\times1)$ and is threefold symmetric. The LEED spots alternate between fuzzy and sharp as a function of the beam energy. A 2.3-ML Fe film has a similar LEED pattern with a brighter background and very broad spots. These LEED patterns indicate that the atoms sit largely in lattice sites but many steps are present. Films that are annealed to 350 K have sharpened LEED spots and a clearer three-fold symmetry. In contrast, the XPS angular anisotropy shows little change in structure for films that are annealed, indicating that short-range order in the films changed little. A film thicker than 4 ML has a LEED pattern that is sixfold symmetric with broad spots. In addition, the LEED pattern has new diffuse spots (these spots are similar to those labeled *B* in Fig. 4, which are observed in room temperature grown films). Annealing the films sharpens the LEED pattern but less so for thicker Fe films. A 5.6-ML film grown at 80 K and

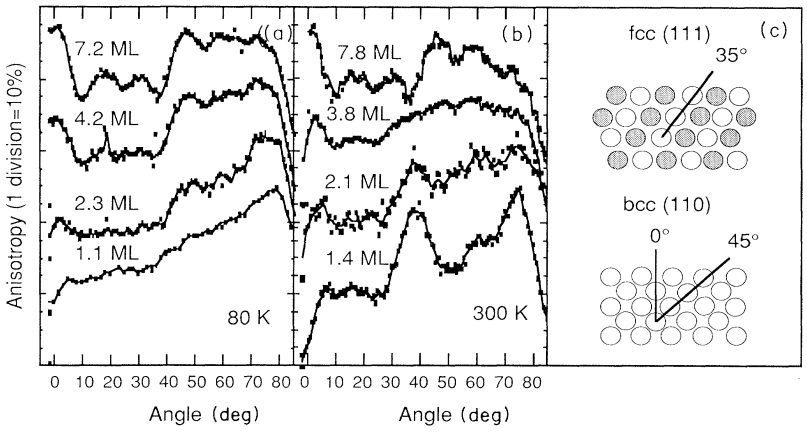

FIG. 3. XPS angular anisotropy for Fe films grown on Cu(111) at (a) 80 K and (b) 300 K using Fe $3p_{3/2}$ photoelectrons. Schematic diagrams indicating directions of scattering enhancement for fcc (111) and bcc (110) are shown in (c). The data were recorded in the $\langle 1\bar{2}1 \rangle$ azimuth of Cu(111). Note that the true bcc Fe $\langle 001 \rangle$ azimuth is 5.3° off this $\langle 1\bar{2}1 \rangle$ azimuth. The shaded atoms lie in a layer below the plane of the page.

briefly annealed to 600 K has a LEED pattern similar to a 6-ML film grown at room temperature.

The films deposited at room temperature, 300 K, show a more complex growth process than the films deposited at low temperature [see Fig. 3(b)]. The XPS angular anisotropy of a 1.0-ML film (not shown) and a 1.4-ML film of Fe show a very strong peak near 37°. The strength and width of this peak suggest a substantial number of Fe atoms have atoms that lie above them. Figure 3(c) demonstrates that fcc(111) should have a peak in the angular anisotropy at 35.3°. Therefore, Fe deposited at 300 K grows in a distorted fcc phase with an approximate interlayer compression of 3–6%. This relaxation is near the previously reported value of 2.5%.[10] A 2.1-ML film has a decreased angular anisotropy. The 37° fcc peak persists in the angular anisotropy, but there is also a broad peak at 0°, which is not found in fcc(111). A 3.8-ML film has an angular anisotropy lacking discernable structure, except a clear peak at 0°. This implies the structure of the Fe film is neither purely fcc nor bcc. It is conceivable that there could be domains of fcc and bcc, and a summation of the anisotropies for the 2.1- and 7.8-ML films produces an angular anisotropy similar to the 3.8-ML film. A 5.8-ML film of Fe (not shown) has an angular anisotropy that indicates the film has converted entirely to a bcc(110) structure. This bcc structure persists for thicker films. Comparing a 7.8-ML film grown at 300 K to a 7.2-ML film grown at 80 K shows that the room-temperature film is similar to the cold film only better ordered as expected.

LEED patterns for room-temperature-grown films also show a gradual transition in structure with increasing Fe thickness. Films less than 2 ML thick have a LEED pattern that is $p(1\times1)$ with broadened spots and a strong threefold symmetry. This pattern corresponds to fcc Fe. Films more than 2 ML thick have a LEED pattern with a pair of weak, elongated spots (labeled *A* in Fig. 4), which develop inside the first-order Cu spots. Increasing the Fe film thickness further decreases the Cu LEED spot intensity and produces an additional pair of LEED spots outside the first-order Cu spots (labeled *B* in Fig. 4) and a spot intermediate between the *A* spots. Films 8 ML thick have the LEED pattern shown in Fig. 4. This pattern can be interpreted as a bcc (110) Fe structure. How-

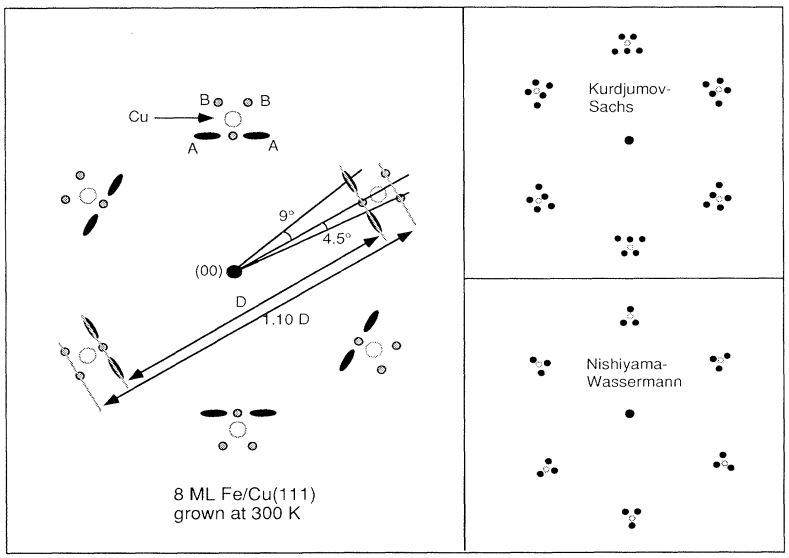

FIG. 4. Schematic illustration of the LEED pattern for an 8-ML film of Fe on Cu(111) grown at 300 K (on left). Illustrative LEED patterns for bcc(110) on fcc(111) with Kurdjumov-Sachs and Nishiyama-Wasser orientations (on right). Six equivalent domains are included for the Kurdjumov-Sachs pattern and three equivalent domains are superimposed for the Nishiyama-Wasser pattern. The Kurdjumov-Sachs orientation is more consistent with observations.

ever, the bcc Fe(110) lattice can assume two different correspondences with the fcc Cu(111) surface net, which are commonly called Kurdjumov-Sachs (KS) and Nishiyama-Wasserman (NW). The KS (NW) orientations correspond to alignment of the fcc(111) dense-packed $\langle\bar{1}10\rangle$ rows of atoms with the bcc(110) troughs along the $\langle\bar{1}11\rangle$ ($\langle 001\rangle$) directions.[98] Also, the hexagonal symmetry of the Cu lattice permits three symmetric orientations for both KS and NW. Using the lattice constants given in Table I and assuming the ideal KS and NW configurations, lattice match for bcc α Fe(110) on fcc Cu(111) will produce a 5.7% Fe contraction for KS or a 8.9% Fe expansion for NW. Therefore, the elastic strain in the Fe film should favor KS over NW. The LEED pattern observed for 8 ML of Fe grown at 300 K is compared to the LEED patterns for KS and NW orientations in Fig. 4. Although the elongation of the *A* spots indicates a deviation from the ideal configurations, the KS orientation is the better choice. The predicted angular separation of the Fig. 4 *B* spots is 10.5° for KS.[77] This estimate compares well to our measured value of 9±1°. Similar measurements made by Gradmann and Tillmanns[80] gave 10°. The diametric ratio of the outer doublet and inner triplet separations should be 1.15 for KS. We find the ratio to be 1.10±0.5. Also, similar LEED patterns have been observed for KS orientations of bcc Fe on hcp Ru(0001) (Refs. 103 and 104) and fcc Ir(111).[104] Therefore, the experimental LEED pattern confirms the alignment is predominantly KS and demonstrates the presence of multiple bcc domains originating from the six equivalent orientations.

In summary, the Fe films grown at 80 K are bcc with an undetermined orientation. While the Fe films grown at 300 K start as distorted fcc(111) and evolves with thickness into a nearly ideal bcc(110) with Kurdjumov-Sachs orientation. This result is in agreement with other reports of bcc(110) Fe that is in the KS orientation on Cu(111).[79,80] We did not observe the NW orientation reported for films grown at 673 K.[78] The evolution of the LEED pattern suggests that the fcc to bcc transformation may not take place as a simple superposition of fcc and bcc domains, since naively this would produce a simple incoherent sum of the appropriate fcc and bcc patterns. Instead, the data suggest that a complex phase transformation occurs over a range of film thicknesses, possibly facilitated by the propagation of bulk misfit dislocations.[75,105,106]

CO-titration experiments are very useful to understand the film-growth process. We mentioned above that the room-temperature Fe growth was not in an ideal layer-by-layer manner and substantial Cu is exposed at the surface. The distribution of the Cu will be reflected in CO-titration measurements taken at angles ranging from near normal to near grazing. This information will help answer the important and difficult questions of whether the Fe is agglomerating, the Cu is segregating, or both.

Figure 5 shows the fraction of Cu in the surface as a function of analyzer angle for ~5.5-ML films grown between 80 and 450 K. The inset in Fig. 5 plots similar measurements for 2.0-ML films grown at 80 and 300 K. The included error bars represent the

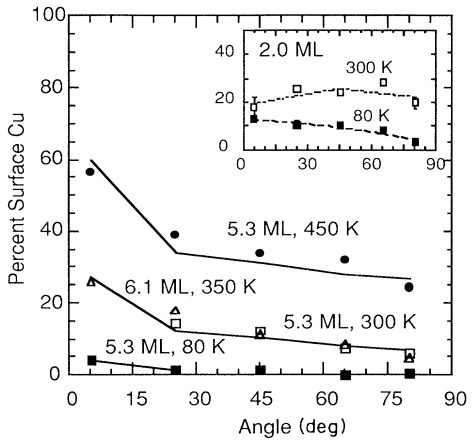

FIG. 5. The fraction of Cu in the surface for Fe deposited on Cu(111) measured using CO-titration technique with varying detection angle. Films approximately 2 ML (inset) and 5–6 ML thick were grown at varying substrate temperatures. Solid squares, open squares, triangles, and circles denote films grown at 80, 300, 350, and 450 K, respectively. Curves show fits to the data using a simple model allowing for visible substrate Cu and segregated Cu (see text). The 6.1-ML film grown at 350 K is fit using 8% segregated Cu and 19% exposed substrate Cu. The 5.3-ML film grown at 450 K is fit using 27% segregated Cu and 33% exposed substrate Cu.

adsorption/desorption sequence as described in Sec. II. The 2.0-ML Fe films show only a weak variation in Cu with detection angle. There is substantially more Cu in the surface for the 300-K deposition than for the 80-K deposition. A 5.3-ML Fe film grown at 80 K shows very little Cu with a small rise toward 0°. Growth of a 5.3-ML film at 300 K and a 6.1-ML film at 350 K show similarly increased Cu distributions with a significant rise near normal. Finally, a 5.3-ML film grown at 450 K displays much more Cu, again with a peak around normal. In general, the fraction of Cu in the surface increases with growth temperature and there is a larger increase for the data collected near the surface normal.

A simple model can be used to understand these data. Since the LEED spots of the film are symmetrical broadening, the film morphology should be azimuthally symmetric on average. We assume a model with a Fe film that may be discontinuous to expose the Cu substrate and allow for segregated Cu to reside above the Fe. The film morphology can be viewed as in Fig. 6. The Cu atoms exposed at the surface will have $2p_{3/2}$ core levels that are shifted by adsorbed CO. The Cu $2p_{3/2}$ photoelectrons emitted from these Cu atoms at the surface can travel unobstructed to the detector or through the Fe layer where they are attenuated. We assume the photoelectrons detected up to 5° off the normal are not attenuated, since perfectly vertical cluster sides are unlikely. The angular-dependent CO-titration signal $S_{\%\mathrm{Cu}}$ (or the fraction of Cu in the surface) for $\theta > 5°$ can then be written as

$$S_{\%\mathrm{Cu}}(\theta) = S_{\%\mathrm{Cu,top}} + S_{\%\mathrm{Cu,bottom}} \exp\left[\frac{-d}{\lambda\cos(\theta)}\right], \qquad (2)$$

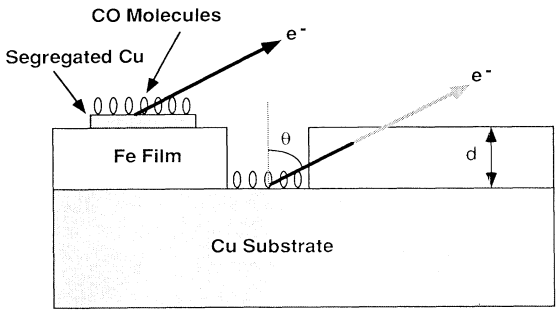

FIG. 6. A schematic illustration of a film morphology that allows for both substrate and segregated Cu. This model is used to interpret angular-dependent CO-titration results. CO adsorbs on exposed Cu (and also on Fe, but is omitted for clarity). Cu $2p_{3/2}$ photoelectrons from substrate are attenuated by Fe overlayer of thickness d before detection.

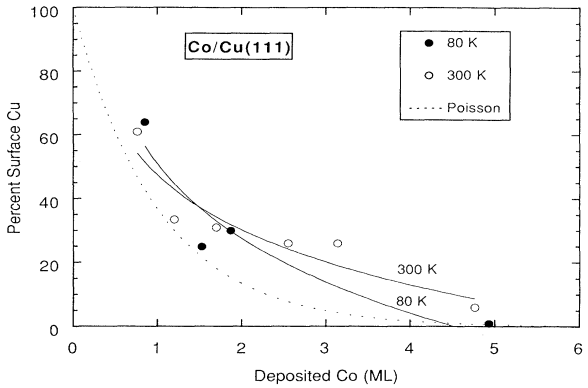

FIG. 7. The fraction of Cu in the surface for Co deposited on Cu(111) at 80 and 300 K. Coverage is determined by CO-titration technique using the average of adsorption and desorption measurements for 25° detection angle. Solid curves illustrate an exponential drop in measured fraction of Cu in the surface. The dotted line indicates the fraction of Cu in the surface for random substrate coverage according to Poisson statistics. The results appear rather insensitive to the growth temperature.

where d is the average Fe film thickness deposited (in Å), λ is the inelastic mean free path [10.5 Å (Ref. 107)], $S_{\%\mathrm{Cu,top}}$ is the fraction of Cu on top of the Fe, and $S_{\%\mathrm{Cu,bottom}}$ is the fraction of exposed substrate. There are no adjustable parameters if we take

$$S_{\%\mathrm{Cu,top}} = S_{\%\mathrm{Cu}}(80°) ,$$
$$S_{\%\mathrm{Cu,bottom}} = S_{\%\mathrm{Cu}}(5°) - S_{\%\mathrm{Cu}}(80°) , \quad (3)$$
$$d = d_{\text{deposited ML}} \times \text{Å per ML} \times (1 - S_{\%\mathrm{Cu,bottom}})^{-1} .$$

Figure 5 shows these fits to the data using a Fe monolayer thickness of 2.05 Å. Despite the simplicity of the model, the agreement is satisfactory. We take this agreement to indicate that the essential morphology is contained in our model. However, it is important to recognize that implicit within this model are the assumptions that the substrate is relatively flat and the width of the gaps in the film is less than or equal to the thickness of the film. Other models may be consistent with the data, but few more simple or more intuitive. This model leads us to conclude that both Fe agglomeration and Cu segregation occur and are important.

B. Co/Cu(111)

Cobalt films up to 5 ML thick were grown at 80 and 300 K. The CO-titration results of the fraction of Cu in the exposed surface are shown in Fig. 7. A substantial fraction of the surface is Cu for the few ML films. More than 50% of the surface is still Cu after deposition of 1 ML of Co, which is comparable to Fe deposited on Cu(111). Unlike Fe/Cu(111), however, the effect of growth temperature upon the fraction of Cu in the surface is small.

Forward-scattering measurements show that films grown at 80 and 300 K are structurally similar. Figure 8 plots XPS angular anisotropies for films grown at 80 and 300 K with thicknesses from 1 to near 5 ML. The film grown at room temperature [Fig. 8(b)] show more pronounced structure in the angular anisotropy, which is expected for better ordering. Both growth temperatures show substantial structure for only ~1 ML of deposited Co. This clear structure indicates that the growth is not simply layer by layer. Comparison of the observed angular anisotropy peaks to the lattice models shown in Fig. 8(c) shows that the Co is stacked both fcc(111) and hcp(0001). If only a single crystalline phase were present, it would be straightforward to determine.[108] However, it is difficult to determine of the ratio of fcc to hcp Co because there is an overlap of the fcc first-order constructive interference with the hcp peak at 55°. The only other forward-scattering peak for hcp Co with our measurement geometry is the weaker 0° peak. Given full polar and azimuthal XPS angular anisotropy profiles, it is potentially possible to resolve uniquely the fcc and hcp components.[109] Nevertheless, the XPS angular anisotropies shown in Fig. 8 suggest that the ratio of fcc to hcp Co fractions is nearly constant for the first 5 ML deposited at either 80 or 300 K. Furthermore, there is a much larger proportion of fcc stacking than hcp stacking in the films grown at room temperature. The strong 0° peak in the angular anisotropy of the 4.9-ML film grown at 80 K is consistent with a significant hcp fraction. In addition, the angular anisotropy of the 4.9-ML film shows a broadening of the 35° peak and about a −3° shift in the 55° peak. The origin of this shift is unclear and could be interpreted as nearly a 7% expansion in the Co hcp interlayer spacing, but this seems unlikely and further study is necessary. A small but significant peak in the angular anisotropy near 0° suggests a small hcp fraction in the 4.7-ML film growth at 300 K.

The Co stacking can also be determined by examining the substrate Cu angular anisotropies. After deposition of a 2.4-ML Co film at 80 K, the substrate Cu anisotropies (Fig. 9) have no detectable peak at 55°, but a 0° peak

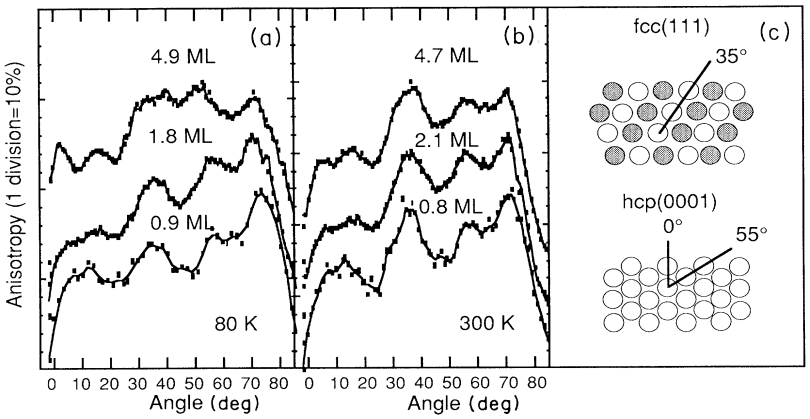

FIG. 8. XPS angular anisotropy for Co films grown on Cu(111) at (a) 80 K and (b) 300 K using Co $3p_{3/2}$ photoelectrons. Schematic diagrams indicating directions of scattering enhancement for fcc(111) and hcp(0001) are shown in (c). The shaded atoms lie in a layer below the plane of the page.

for Cu 3*s* (1362 eV), Cu $3p_{3/2}$ (1409 eV) [not for Cu $2p_{3/2}$ (552 eV) and Cu *CVV* (916 eV)] and a weak peak near 14°. The 14° peak shown in Fig. 9 is not distinct in the clean substrate angular anisotropy, although the weaker, first-order constructive interference peak falls near here [see Fig. 1(c)]. This structure in the Cu XPS angular anisotropy can be understood as the scattering off the third hcp Co layer from the interface Cu layer compounded by interference, which is typical of long source/scatterer separations.[69] We conclude that the interfacial Co maintains the fcc stacking with respect to the Cu lattice as indicated by the absence of a 55° peak in the angular anisotropy. The second Co layer stacks both fcc and hcp with respect to the Cu. The third Co layer continues hcp or the Cu fcc, and a significant fraction of the stacking faulted Co fcc phase is excluded by the lack of a 19.5° peak in the Co XPS angular anisotropy. Therefore, the Co may have two possible hcp stackings and one fcc stacking [Fig. 10(c)]. The two hcp stackings, *BAB* and *BCB*, can be differentiated by a 0° peak in the Cu XPS angular anisotropy for 2 ML of Co or in the Co XPS angular anisotropy for 3 ML of Co. Since no 0° Cu peak is detected for 2 ML of Co, the hcp stacking is predominantly *BCB*.

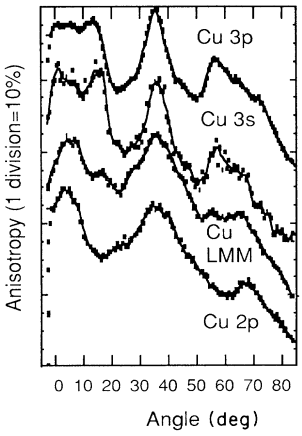

FIG. 9. XPS angular anisotropy of substrate Cu for a 2.4-ML Co film grown on Cu(111) at 80 K. Note increasing intensity at 0° and 15° with increasing Cu energy. Anisotropies are used to interpret stacking of Co phases (see text).

These findings are in very good agreement with recent x-ray scattering studies of Co/Cu(111) superlattices grown on GaAs(110).[90] These results, for growth temperatures of 323 K, found that Co stacking coherence was maintained for thicknesses up to 20 Å with a constant hcp fraction of 35% up to 40 Å.

To examine the stability of the hcp phase relative to the fcc phase for Co/Cu(111), a 2.4-ML film was grown at 80 K and progressively annealed. Figure 10(a) plots the evolution of the XPS angular anisotropy with brief (10 s) anneals to temperatures up to 900 K. From 80 to 530 K, the angular anisotropy shows a small, gradual increase in the fcc 35° peak relative to the hcp 55° peak. The angular anisotropy of the film after a 700-K anneal shows a drop at 0° and nearly equal 35° and 55° peaks. Only after annealing the film to 900 K does the XPS angular anisotropy look comparable to fcc Cu(111) [see Fig. 1(c)]. Figure 10(b) shows the normalized maximum peak intensities and integrated areas of the Fig. 10(a) angular anisotropy scans versus annealing temperature. The peak intensities and the integrated areas show nearly the same

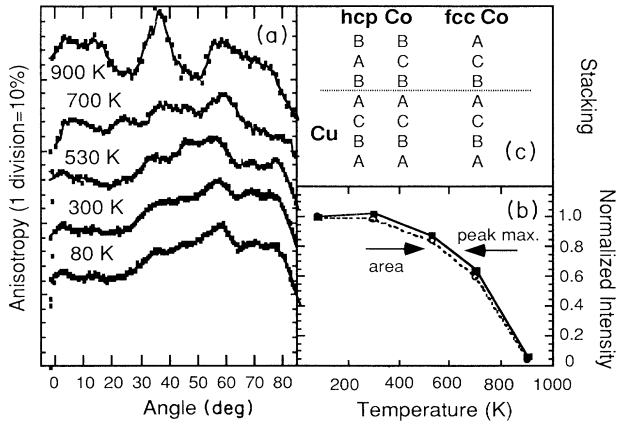

FIG. 10. (a) XPS angular anisotropy for 2.4-ML Co film grown on Cu(111) at 80 K and briefly annealed to the indicated temperature. Spectra were measured using Co $2p_{3/2}$ photoelectrons. The peak maximum intensity and angular integrated intensities of (a) are shown in (b). Diffusion becomes prominent near ~500 K. (c) shows possible Co layer stacking on Cu(111); see text for discussion.

decay with annealing temperature. The lines shown are spline fits and serve primarily as guides to the eye, but they suggest that small deviations in Co signal strength from the as-grown film begin about 400 K. Annealing to 530 K shows about a 15% drop in Co signal strength and only minor changes in the structure [Fig. 10(a)]. Annealing to 700 K shows around a 40% drop and 900 K an abrupt ~95% decrease in Co signal strength. The slow drop of the Co intensity with annealing is consistent with the bulk immiscibility of Co and Cu [fcc Co is estimated to have a bulk solubility of 0.10% Cu at 695 K (Ref. 10)]. In addition, it is also worth noting that bulk Co undergoes a martensitic phase transition from hcp to fcc at 697 K,[111] although it is believed that this temperature may be lowered by the addition of Cu. Therefore, Figs. 10(a) and 10(b) show that the fcc Co phase is dominant only when substantial bulk interdiffusion of Co and Cu has occurred. The hcp stacked Co is remarkably stable since this 2.4-ML Co film, about a single unit cell, displays only small changes until bulk diffusion is important. The Co *BCB* hcp stacking differs from the *BCA* fcc stacking by only the top layer. Conversion from hcp to fcc Co should occur at temperatures where surface diffusion of the top Co layer is significant, but this is not the case and the structure is frozen well above room temperature. Therefore, the hcp stability may be attributed to a segregated Cu layer that forms above room temperature and drives the fcc to hcp transition up toward bulklike temperatures.

The LEED patterns of films of Co on Cu(111) are generally $p(1\times1)$. Growth at 80 K produces films that have broader spots and moderately higher backgrounds than films grown at 300 K. Co films up to 3 ML thick have LEED patterns that show a diminishing threefold symmetry with increasing thickness. After deposition of ~3 ML of Co, the threefold symmetry of the LEED pattern is lost completely, but it can be restored by annealing the films.

C. Discussion

Our results show that varying the growth temperature between 80 and 300 K has profound effects upon the film morphology and crystallographic structure for Fe on Cu(111), but only weak effects for Co on Cu(111). This effect can be elucidated by examining the role of the substrate growth temperature upon the film growth kinetics. A useful measure of the significance of substrate growth temperature is provided by estimation of adatom surface diffusion. The activation energies for surface diffusion have been measured for a number of metal surfaces using field-ion microscopy (see Refs. 28–33 and references therein). Unfortunately data are not available for Fe and Co, but good estimates of self-diffusion activation energies can be obtained by scaling experimental results with cohesive energy as described in the Introduction. Table II gives the estimated surface activation energies and the mobility in hops/s assuming an Arrhenius behavior. The activation energy is significantly more for both Co and Fe than for Cu. Table II shows the mobility of the Cu atoms at 80 K is considerable, while the Co and Fe are predicted to diffuse relatively little. At 300 K, all three atomic species are predicted to be very mobile and a single adatom could sample a small but significant fraction of the surface (roughly 0.001% or 10^{12} sites) in a single second. It is important to recognize that the values given in Table II are for self-diffusion, *A* on *A*. The activation energy for dissimilar elements, *A* and *B*, is generally not trivially related to the individual self-diffusion barriers.[28] Although, recent molecular-dynamic simulations and transition state theory calculations[12] for the (100) face of fcc transition and noble metals suggest that the system of *A* on *B* may be at least crudely approximated by *A* on *A*.[13]

At 80 K, the growth of Fe/Cu(111) is not in an ideal layer-by-layer manner. Deposition of the first monolayer covers much of the substrate and the surface is about 25% Cu. After 2 ML of Fe is deposited, the surface is about 15% Cu. Angle-dependent CO-titration results suggest little or no Cu (~4%) resides on top of the Fe with about 12% of the Cu substrate exposed. After 5 ML of Fe is deposited, the surface is about 5% Cu, which can be attributed entirely to deep, narrow channels in the Fe overlayer that expose the substrate. Presumably the sides of these channels are the steep close-packed ⟨111⟩ planes. Overall there appears to be a weak tendency for Fe not to wet the surface even at 80 K. Cu surface segregation may be present at 80 K but barely detectable. The first Fe ML is lattice matched to the Cu. By the third ML the Fe is bcc and laterally contracted with respect to the Cu surface. As the Fe film thickness increases, disorder grows quickly in the LEED, but the local order measured by forward scattering remains clear. Annealing a 5.6-ML film to 600 K produces a film with a good LEED pattern. The annealed film is bcc with predominantly Kurdjumov-Sachs oriented domains.

Compared to growth at 80 K, Fe films grown at 300 K show a significantly larger fraction of the surface is Cu for all film thicknesses. Also, there is a complex Fe phase change with increasing film thickness. After 2.0 ML of Fe is deposited, the surface is about 25% Cu. Forward

TABLE II. Estimated surface self-diffusion of Cu(111), Fe(111), and Co(111). Activation energies for Cu(111), Fe(111), and Co(111) are scaled from Ir(111) (Ref. 30) according to cohesive energy (Ref. 54). Mobilities are determined using an Arrhenius diffusion law with a preexponential of 10^{-3} cm^2/s (Refs. 28, 29, and 32).

Surface	Activation energy (eV)	hops/s 80 K	hops/s 300 K	hops/s 450 K
Cu/Cu(111)	0.14	10^4	10^{10}	10^{11}
Fe/fcc Fe(111)	0.18	50	10^{10}	10^{11}
Co/fcc Co(111)	0.19	10	10^{10}	10^{11}

scattering and LEED measurements show that the Fe is fcc, strained to match the Cu lattice pseudomorphically. Increasing from 2 to 6 ML of deposited Fe produces a slow drop in surface Cu and a transition from fcc to bcc Fe. After 6 ML of Fe is deposited, 15–20 % of the substrate is still uncovered and angle-dependent titration results indicate ~5% segregation. These data suggest that the Fe phase change correlates with an increasing substrate coverage. Compared to the 80-K films, we see that the Fe tends to agglomerate more strongly at the higher growth temperature. This claim is also supported by increasing the growth temperature to 450 K, which results in nearly 30% exposed substrate for 6 ML of Fe. In addition, surface segregation of the Cu becomes more prominent with increasing substrate growth temperature. It is reasonable to expect that higher temperatures would continue to promote this trend.

Indeed, Fe films prepared at 673 K are reported to nucleate as three-dimensional fcc clusters strained to match the Cu lattice.[75] Furthermore, the bcc phase was not observed until almost a continuous Fe film was formed, which is consistent with our observations. Recently the Fe/Cu(111) system has been studied by STM.[99] This STM study found that a 3-ML Fe film grown at 420 K consisted of isolated islands, typically 100 Å in diameter, separated by narrow channels. If we estimate from our own results that 30% of the Cu substrate is exposed for a 3-ML film grown at 420 K and assume roughly circular islands, one finds that the channels should be about 7 Å wide and 7 Å deep, which is consistent with our model. This STM study also reported that about 10% of the Cu substrate was still exposed after deposition of about 4 ML of Fe at 300 K. Our CO-titration measurements indicate about 17% of the substrate is exposed after an equivalent deposition. Therefore, the STM results fit very well with the simple model and the growth mode we presented above.

We can understand the Fe film morphology in terms of surface diffusion and agglomeration, which increase with growth temperature (Table II). At 80 K, the Fe mobility should be low and the Fe covers most of the surface quickly, if it sticks near to where it lands. At higher temperatures, the Fe mobility is greater and the atoms can diffuse many lattice constants from the incident site before stopping. Since the Fe surface free energy is higher than the Cu surface free energy[3,54] and the Fe-Cu interface energy is unfavorable to layer-by-layer growth,[54] the equilibrium growth mode should correspond to the observed Volmer-Weber type of growth.[2] The situation is compounded by surface segregation of the Cu substrate for higher growth temperatures, but this appears to be a less important factor.

Our results show that varying the growth temperature between 80 and 300 K for Fe on Cu(111) has profound effects upon the film morphology. We propose that the changing film morphology effects the crystallographic phase. The smaller island clusters are coherent with the substrate. Only when the islands are very large does the Fe relax into its bcc ground state. It is not surprising that this complex growth mode may be misinterpreted, if one believes that the growth is ideal layer by layer. One would then be led to believe that the increasing film thickness produces a homogeneous strain that is relieved by the continuous Fe film "breaking with" the substrate and becoming bcc. Instead these data suggest the individual islands and groups of islands must reach a critical size, which then precipitates the transformation.

The subtleties of bcc(110)/fcc(111) epitaxial growth are discussed by Bauer and van der Merwe.[98] One must include the film/substrate bond strength, as well as the intrafilm interaction strength to ascertain the film epitaxial phase. For Fe on Cu(111), Bauer and van der Merwe find that the Fe may grow either bcc with KS orientation or pseudomorphically depending upon the intrafilm interaction strength compared to the interface bond strength. Our results can be explained as a changing balance between these interaction strengths, which depends upon the film thickness and the island size.

It is now appropriate to examine the Fe/Cu(111) growth mode LEED study of Gradmann and Tillmanns.[80] Figure 11 reproduces their basic result: the transition from pseudomorphic fcc Fe to bcc Fe occurs at a film thickness determined by the substrate growth temperature and to a lesser degree by the growth rate. Our results are overlaid in Fig. 11 with lines to describe the trends for low to intermediate temperatures. The agreement is good.[114] The change in behavior apparent in Fig. 11 above 500 K can be explained by the introduction of new diffusion processes. If we consider a single unit cell, we see that these results are consistent with no fcc phase for films grown at 80 K or below. If the structural transitions occur when the islands reach a certain size, the top and bottom curves in Fig. 11 must indicate this transitional thickness. Comparing to the substrate coverage estimates for Fe/Cu(111) (Fig. 2), the bottom and top curves appears to correspond to about 65% and 80% coverage of the substrate, respectively. This observation

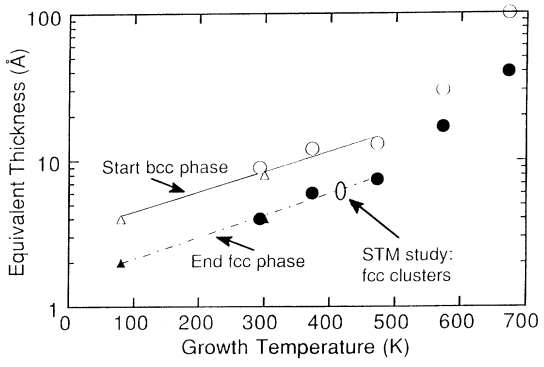

FIG. 11. Crystalline phase diagram of Fe/Cu(111) that plots Fe deposition vs growth temperature. Fe deposition is plotted using the equivalent thickness of flat homogeneous layers. Triangle data points were determined from forward scattering and LEED measurements; see text. Circles indicate LEED results from Gradmann and Tillmanns (Ref. 80). The STM measurement was reported by Brodde and Neddermeyer (Ref. 99). Lines denote approximate boundaries between crystallographic regions: fcc(111) Fe, transitional Fe phase, bcc(110) Fe.

supports the proposal that the fcc to bcc transition occurs at a certain cluster size. Finally, we recognize that both curves displays similar behaviors. Assuming we can write the transitional thickness dependence as a rate equation $d = d_0 \exp(T/T_0)$, we find $T_0 = 295$ K, $d_0 = 1.50$ Å and $T_0 = 330$ K, $d_0 = 3.10$ Å for the bottom and top curves, respectively. The characteristic thicknesses d_0 for substrate coverage and bcc phase formation differ by about a factor of roughly 2 for temperatures up to 500 K. The temperature of $T_0 \sim 300$ K appears to be related to formation and coalescing of the Fe clusters. Simulations are necessary to explore and understand this mechanism, but T_0 may be characteristic of processes of cluster maturation that have been observed using STM.[29]

The crystalline growth mode of Co on Cu(111) was also shown to be regulated by the growth temperature. However, the CO-titration results imply a weaker growth-temperature dependence for Co agglomeration than for Fe. One may suggest that Table II of self-diffusion activation energies suggest the opposite situation, with a more dramatic temperature dependence for Co than Fe, but these estimates are only approximate, especially when applied to dissimilar species (i.e., Co/Cu and Fe/Cu).

The forward-scattering results for Co/Cu(111) suggest a more complex picture than the CO-titration alone. We showed above (Fig. 8) that the 80-K grown films contain a larger fraction of hcp than fcc stacked Co compared to the 300-K grown films. Furthermore, this proportion appears roughly constant, independent of film thickness up to 5 ML. The similarity between the 1- and 5-ML Co films grown at 300 K argues against any substantial Cu surface segregation, which should diminish quickly with thickness. Therefore, the strong XPS angular anisotropy observed already in the ~1-ML-thick Co films and the large fraction of Cu in the exposed surface, ~60% for 1 ML of Co, implies that the Co is clustering at both 80 and 300 K. The lack of a good 0° peak for Co thicknesses less than 3 ML indicates that at least the hcp fraction is completing the first two layers before the third layer starts. There is no similar peak for the fcc fraction to distinguish the two and three layer proportions.

We have demonstrated that the hcp/fcc ratio depends on the film-growth temperature; however, one must inevitably ask why this is the case. Again, considerations of surface diffusion can offer an explanation. The initial agglomeration of Co requires a high mobility of Co on the Cu(111) surface so that the adatom can preferentially diffuse to a nearby cluster and be included. Evidence for this mobility is provided by the similarity of the substrate coverage at 80 and 300 K (Fig. 7) and the lack of stacking faulted Co in the first monolayer, which would be equally populated by random deposition. Once incorporated, the Co mobility may be markedly reduced as suggested by Table II, particularly at 80 K. The mechanism for incorporation at an ascending step will be manifested in the Co second layer structure. A recent study of Ir and W on Ir(111) suggests an interesting view of this phenomena.[33] The Co is expected to nucleate like Ir/Ir(111) as small close-packed clusters with edges perpendicular to the $[\bar{2}11]$ symmetry directions.[115] An approaching Co adatom can be included into the cluster either by a single hop to a second layer site in keeping with standard ideas of crystal growth, or by a concerted exchange of the adatom and a cluster atom.[33] The displaced cluster atom may rise to either a fcc or an hcp stacked site.[116] Given that the mobility of the second layer Co atom at a step edge will be much reduced compared to its mobility on a flat (111) surface, we expect from Table II that the edge atom is effectively frozen in place at 80 K. The substantial hcp fraction for the 80-K films can therefore be taken as evidence for an incorporation mechanism whereby the second layer atom resides in the hcp site. Verification of this scenario, which has been previously proposed for Ir/Ir(111), is subject to future work. Increasing the growth temperature or annealing the film will permit the second layer atoms to diffuse more easily from its initial site to a fcc site. This can explain the larger fcc/hcp fraction for 300-K grown and annealed films. We have no evidence for a second bilayer after the first two layers are completed, which is also dictated by the low mobility of Co/Co(111) at 80 K. Therefore, the relative thickness independence of the hcp/fcc ratio suggests that the initial stacking is maintained for many more layers.

As demonstrated above (Fig. 10), the hcp Co phase is very stable. Figure 12 shows the XPS angular anisotropy of 2.1-ML Co film as-grown at 300 K and after annealing to 400 K for 45 min. There is an increase in the 37° peak with annealing, but no change in the 57° peak. CO titration indicates an ~15% increase in Cu at the surface. Integrated areas of the XPS angular anisotropy show a 40% increase in Cu $2p_{3/2}$ signal intensity and a 47% decrease in Co $2p_{3/2}$ signal intensity. These data suggest that Cu is segregating to the surface and covering the Co.

To investigate further the role of substrate surface structure in Co film growth, we sputtered the Cu substrate with 1500-eV Ne^+ ions at 300 K but did not anneal the surface. The LEED showed broad, threefold sym-

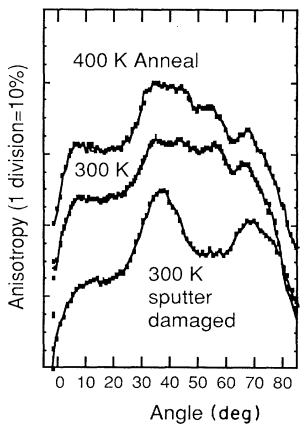

FIG. 12. XPS angular anisotropy of Co $2p_{3/2}$ for a 2.1-ML Co film grown on Cu(111) at 300 K, and after a 45-min anneal at 400 K. Also shown is the XPS angular anisotropy of a 2.1-ML Co film grown at 300 K on a sputtered but unannealed Cu(111) surface.

metric spots before and after a 2.1-ML Co films was deposited at 300 K. Figure 12 shows the XPS angular anisotropy for the film. The very strong and broad 37° peak with no 57° peak in the angular anisotropy indicates the Co must be a distorted fcc. CO-titration measurements for a similar 2.5-ML film shows the exposed surface is still 80% Cu. Integrated XPS intensities form the XPS angular anisotropy shows a 10% drop in the Cu Auger signal strength and a 64% drop in Co 2*p* signal strength compared to our standard sputter-annealed substrate. Not surprisingly, the very rough Cu surface strongly perturbs the Co film-growth kinetics. The film-growth process appears to be complicated, but the heavily stepped Cu surface probably promotes fcc Co through step edge nucleation. Annealing the rough Co film to 500 K results in a film that has sharpened LEED spots along with weak indications of sixfold symmetric faceting.

Recent NMR studies of Co/Cu multilayers with [111] texture grown on SiO_2 found that room-temperature-grown Co films were almost entirely fcc.[85,87] Our single-crystal results show a small hcp fraction and those of multilayers grown on GaAs(110) (Ref. 90) showed a large hcp fraction. The NMR studies also report that the Co/Cu interface is mixed (or rough) with a total width of 2 (Ref. 85) −6 ML (Ref. 87) for each Co layer.[117] The unannealed substrate result (Fig. 12) shows that the observed differences in Co stacking may result from different substrate roughnesses. The high step density of the rough surface promotes fcc stacking through predominantly step edge growth. Low-step-density substrates produce some hcp stacking through growth that occurs via cluster nucleation.

IV. GROWTH OF Fe AND Co ON Cu(100)

The growth of Fe and Co on Cu(100) has been the subject of extensive investigation. The results of different studies have at times appeared contradictory but are largely attributable to variations in preparation procedures and inadequate structural characterization. Recently, a strong motivation has been to understand and control the technologically promising magnetic properties of these systems, such as perpendicular magnetizations[18] and exchange coupling.[119] The fulfillment of this goal is a primary motivation of this work.

The voluminous nature of the Fe/Cu(100) and Co/Cu(100) literature forces an economical review and we will confine ourselves predominantly to single films on single-crystal substrates. Structural studies of Fe/Cu(100) (Refs. 11–13, 16, 17, 57, 62, 66, 67, 74, 77, 105, and 120–133) established as early as 1959 that fcc Fe could be stabilized on Cu(100). Not until 1987 did these studies report that the growth mode was not layer by layer. Variation in film preparations and growth assessment has resulted in reports of the metastable fcc Fe magnetic properties as paramagnetic,[134] antiferromagnetic,[135] or ferromagnetic with possibly different spin phases,[14,15,130,136–142] and a strong perpendicular magnetic surface anisotropy.[118,143–146] Co epitaxially grown on Cu(100) also forms a metastable fcc structure.[147] At substrate temperatures from 300 to 450 K, growth has been reported to be layer by layer[18–23] until recently.[58,70,71,148,149] The reports of Co/Cu(100) ideal film growth has made this system the focus of many magnetic studies.[22,58,137,139,148,150–158] One motivation for this work has been the role of film thickness in reducing the system Curie temperature. Reports of ferromagnetic monolayers[139,150,152] have not been reproduced.[22,58,156,157] Again, the controversy in magnetic properties makes closer attention to structural characterization essential and timely.

The epitaxial lattice match of Fe and Co on Cu(100) is given in Table III. For completeness we list the best fcc and bcc matches for Fe and Co. Clearly the pseudomorphic match is much better for the fcc phase in both cases. However, the bulk bcc Fe and hcp Co phases will be dominant in very thick films.

A. Fe/Cu(100)

Fe films were grown at substrate temperatures of 80 and 300 K. Structural determinations were made from extensive measurements using CO titration, XPS forward scattering, LEED, and RHEED.

CO-titration results for Fe films up to 6 ML are shown in Fig. 13(a). The fraction of Cu in the exposed surface is given for the adsorption cycle (the clean film minus the CO-saturated film) and desorption cycle (the film warmed to 300 K to desorb CO minus the CO-saturated film) of the CO-titration measurements. Unlike the films grown on Cu(111) that typically showed only a 5% variation between adsorption and desorption cycles, the Fe films grown on Cu(100) show a consistent increase in the fraction of Cu in the exposed surface between adsorption and desorption cycles. Fe films grown at 80 K often show a 10–20 % absolute increase in surface Cu and films grown at 300 K generally show a 5–10 % absolute increase in surface Cu. The origin of the increase in surface Cu between adsorption and desorption cycles is uncertain, but may be due in part to Fe agglomeration and possibly Cu segregation during the 300-K-anneal of the CO-titration procedure. To examine the effects of annealing without

TABLE III. Epitaxy of Fe and Co on Cu(100).

Material/ symmetry	Lattice constant (Å)	Nearest neighbor (Å)	Surface cell mismatch (%)	Interlayer spacing (Å)
fcc Cu(100)	3.615	2.55		1.805
fcc Fe(100)	3.59	2.54	−1.1	1.795
bcc α Fe(110)	2.87	2.48	−10.6	2.03
fcc Co(100)	3.54	2.50	−3.9	2.05
bcc Co(110)	2.82	2.44	−13.8	1.99

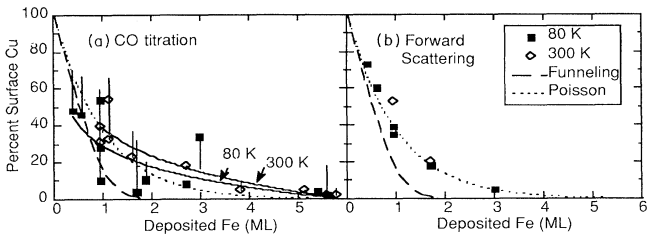

FIG. 13. The fraction of Cu in the surface for Fe deposited on Cu(100) at 80 and 300 K. (a) shows Cu values determined by CO-titration technique using a 25° detection angle. (b) shows Cu values determined by XPS angular anisotropies. Solid squares and open diamonds indicate as-grown measurements for growth temperatures of 80 and 300 K. Error bars indicate changes for desorption titration cycle. Solid curves show exponential fits to the as-grown data. Dashed and dotted curves show the fraction of Cu in the surface for predictions based upon downward funneling and Poisson random deposition models.

adsorbed CO, a 0.9-ML Fe film grown at 80 K, then annealed to 300 K, gave adsorption and desorption values of 38% and 50%, respectively. This compares very well to a similar film grown at 300 K and indicates that annealing an 80-K monolayer to 300 K produces results comparable to growth at 300 K. A 0.9-ML film grown at 80 K and annealed to 375 K showed a substantial increase in surface Cu to 66% and 87% for the adsorption and desorption titration cycles, respectively.

Particular attention was paid to Fe depositions near 1 ML. Three one-monolayer films were grown at 80 K and measured during the course of this study. The substantial variation in adsorption results shown in Fig. 13(a) can be correlated with changes in the Cu substrate. Table IV lists the results. The 54% value was obtained soon after start of the experiments. The 10% value was measured a few days later, and had a 12-ML Cu buffer layer grown at 600 K prior to the Fe. The intermediate value of 28% was measured three weeks (and approximately 30 films) later using the same substrate with no buffer layer. We do not believe these changes are due to impurities because all the films were free of contamination as measured by XPS. Although trace impurities (<0.01 ML) cannot be completely ruled out, they should not dominate the kinetics at growth temperatures were adatom mobility is very low (i.e., 80 K). The substantial changes in film growth are caused by apparently subtle changes in the substrate quality.

To understand the role of the surface steps and defects, we measured the surface Cu for a 1.0-ML Fe film deposited at 80 K on a sputtered and unannealed substrate. The CO titration showed the surface Cu was only ~2%. This surprising result suggests that the observed titration variations may be due to changes in surface defects and roughness. This very low percentage of surface Cu may be attributed to nearly perfect coverage of the substrate by the Fe. However, the forward-scattering anisotropy for the film deposited on the unannealed substrate shows a significant 45° peak indicating second-layer formation, which makes the 2% result suspicious. Alternatively, we can speculate that the high density of defects and steps trap the Fe adatoms near where they land, producing many small clusters. These smaller, more populous Fe islands may act to block a high proportion of adjacent Cu sites from CO adsorption, resulting in an underestimate of exposed copper compared to a more ideal surface. Further evidence for some substrate blocking is given by the result of 48% surface Cu for only 0.37 ML of deposited Fe at 80 K using a 18-ML Cu buffer layer (since $0.48+0.37=0.85$ not 1.0). However, a 0.56-ML Fe deposition, without a buffer layer, yields 46% Cu ($0.56+0.46=1.0$). (Forward-scattering data discussed below will also favor the blocking interpretation.) These results imply that the substrate defect density changes significantly as the crystal is used for experiments and

TABLE IV. CO-titration results for exposed Cu(100) with varying substrate preparations and growth temperatures.

Deposition	80-K growth adsorption cycle (% Cu)	80-K growth desorption cycle (% Cu)	300-K growth adsorption cycle (% Cu)	300-K growth, desorption cycle (% Cu)	Substrate preparation
0.93 ML Fe	54	50	33	66	standard, day 1
0.93 ML Fe	10	39	31	58	12 ML Cu buffer layer grown at 600 K, day 4
0.93 ML Fe	12	35	40	60	standard, day 20
1.0 ML Fe	2	50			sputter damaged, day 20
2.8 ML Fe	34	17			standard, day 1
2.8 ML Fe	8	9			standard, day 9
0.85 ML Co	43	45	33	75	standard, day 3
0.85 ML Co	7	43			12 ML Cu buffer layer grown at 600 K, day 8
0.85 ML Co	20	42	56	62	standard, day 22
0.85 ML Co	14	41			sputter damaged, day 8

with the addition of a Cu buffer layer at 600 K (see Table IV). However, it is not clear how the decrease in apparent surface Cu for films grown on the buffered substrates should be interpreted. It seems counterintuitive that the crystal that has been repeatedly sputtered and annealed and the crystal that has a homoepitaxed buffered layer should have similar morphologies. It is conceivable that growth on the stepped and buffered substrates could be dominated by different processes such as surface diffusion and agglomeration. Nevertheless, these imperfections are most important for the cold grown films when surface diffusion is most easily restricted (see Table III). This can be demonstrated by warming the ~1-ML films to 300 K and repeating the CO titration for the second step of the cycle (desorption). In all cases, this produces comparable results of 50%, 39%, 35%, and 50% (see Table IV). Furthermore, films grown at 300 K do not show the same dramatic changes with substrate quality. Approximately 1-ML films grown at 300 K on the same days as above and under identical conditions, except growth temperature, yield similar adsorption (desorption) values of 33% (66%), 31% (58%), and 40% (60%) Cu in the surface. Finally, substrate imperfections may also be important for thicker films (Table IV). Figure 13(a) shows two films approximately 3 ML thick grown at 80 K. The larger value of 34% Cu in the surface was measured on the same day as the first 1-ML Fe film, while the 8% value was measured one week later. After warming to 300 K, both films gave closer agreement with readings of 17% and 9%, which indicates more similar film morphologies after annealing. If defects and steps trap Fe adatoms, the implications of these results is that even larger values of surface Cu would be obtained for Fe films deposited on truly perfect Cu(100) where mobility is not inhibited by steps.

Figure 13(a) of surface Cu versus deposited Fe shows a general decrease in surface copper with decreased growth temperature and increased Fe deposition. The Fe growth is not simple layer by layer below 5 or 6 ML. Table V of surface diffusion activation energies shows that Fe adatoms should be effectively frozen in place at the 80-K growth temperature. From this one might expect that the deposited Fe atoms will stick where they land and randomly fill the lattice sites. The resulting fcc (100) film will resemble a Poisson distribution of layered vacancies.[159,160] The percent vacancy of the first layer, or equivalently the percent surface Cu, according to Poisson statistics for a simple cubic lattice is shown by the dotted line in Fig. 13. The titration estimate of surface Cu for growth at 80 K is often less than the Poisson prediction for the thinnest films, while thicker films and those grown at 300 K show generally more Cu. The CO-titration results suggest that the deposited Fe atoms are mobile, even at 80 K. Supported for this view is given by the observation of RHEED oscillations for several systems including Fe/Cu(100) and Cu/Cu(100) at 77 K,[161] since oscillations are not present in the nondiffusive model.[160] To explain the persistence of RHEED oscillations at temperatures where thermal diffusion is believed to be negligible, at least two mechanisms of transient mobility have been suggested. The first proposal of "horizontal" transient mobility[161] is that the latent heat of condensation of the impinging Fe atoms (~3 eV) permits the adatoms to overcome the diffusion energy barrier and briefly diffuse. This energy dissipates after only a few hops according to momentum conservation. However, molecular-dynamic simulations do not support the horizontal transient mobility mechanism; instead, the substrate appears to be elastic and absorbs the energy upon impact.[162,163] The second proposal of "vertical" transient mobility is referred to as downward funneling.[162] This mechanism postulates that the growth front of the fcc(100) film is comprised of many tiny (111) microfacets where the adatoms are funneled down into lower fourfold hollow sites. This model predicts 85% and 99.9% substrate coverage for 1- and 2-ML depositions at 0 K and little change in coverage for temperatures where thermal diffusion is inoperative.[164] The downward funneling prediction is shown by a dashed line in Fig. 13. The CO-titration and forward-scattering results show more Cu than the funneling model predicts. This discrepancy between the measured and predicted surface Cu can be partially attributed to the unwarranted assumption of zero adatom mobility at 80 K. Recent spot-profile analysis LEED (SPA-LEED) studies have shown that the condensing adatoms have sufficient mobility, even at 80 K, to nucleate islands with an average separation of about ten atoms.[102] This short-range correlation indicates that the substrate coverage is not purely random and the probability of an adatom landing in a second-layer site above a complete, four first-layer atoms will be greater. Therefore, the percent surface Cu should increase from the fun-

TABLE V. Estimated surface self-diffusion of Cu(100), Fe(100), and Co(100). The activation energy for Cu/Cu(100) is an experimental average result (Refs. 49–51). Fe(100) and Co(100) activation energies are scaled from Cu(100) according to cohesive energy (Ref. 54). Mobilities are determined using an Arrhenius diffusion law with a preexponential of 10^{-3} cm^2/s (Refs. 28, 29, and 32).

Surface	Activation energy (eV)	hops/s 80 K	hops/s 300 K	hops/s 450 K
Cu/Cu(100)	0.38	10^{-11}	10^{7}	10^{8}
Fe/fcc Fe(100)	0.46	10^{-16}	10^{5}	10^{7}
Co/fcc Co(100)	0.49	10^{-18}	10^{4}	10^{7}

neling model prediction toward the simple cubic Poisson model prediction, as observed.

Variation in the surface Cu with small changes in substrate perfection makes precise characterization of the growth dynamics very difficult. However, we show that a qualitative fit to the data can be obtained by assuming an exponential decrease of the surface copper with deposited Fe. Figure 13(a) shows these fits as solid curves for the as-grown films at 80 and 300 K, respectively. (Similar curves may be fit to the Cu values obtained for the CO-titration desorption cycle, but have not been included for clarity.) Substrate coverage, $<5\%$ Cu, occurs near 4 ML for growth 80 K and near 5 ML for growth at 300 K. Note that previous estimates for substrate coverage was ~ 5 ML for growth at 255 K.[59] Also note that the 300-K curve is similar to the 80-K curve but displaced to the right by ~ 0.5 ML. This suggests that on average the Cu coverage at 300 K approximately lags the coverage at 80 K by 0.5 ML of deposited Fe.

To investigate the distribution of the Cu, we made angular-dependent CO-titration measurements as previously described for Fe/Cu(111). Figure 14 shows the results for a 1.1- and a 5.1-ML Fe film grown at 300 K. Unlike the results for Fe/Cu(111), the 5.1-ML (100) film shows very little Cu, irrespective of detection angle. The (100) fcc Fe film morphology is distinctly different from the (111) fcc Fe films. The surface Cu is limited to a small segregated fraction, $\sim 3\%$. The 1.1-ML film shows a small variation with detection angle. However, it is not prudent to model this variation using the simple model applied earlier, since little Cu $2p_{3/2}$ attenuation can be expected from such a thin film. We simply note that near normal we see $\sim 50\%$ Cu.

XPS angular anisotropies for Fe films grown at 80 and 300 K are shown in Figs. 15(a) and 15(b), respectively. The different growth temperatures show small but significant changes in the XPS angular anisotropies. The structure of these films can be separated into a thin, 1–2 ML-thickness range, and a thick, ≥ 3 ML, thickness range.

The Fe films of three or more monolayers in Fig. 15 show strong peaks in the XPS angular anisotropies near 45° (dashed lines) and a growing intensity near normal. Small angular shifts in these peaks indicate a small but important departure from ideal fcc stacking. The angular anisotropies of films grown at 80 K compared to those grown at 300 K show broadening peaks and decreasing structure, which indicates slowly growing disorder in the cold films. Substantially thicker films, up to 30 ML, grown at 300 K have been studied by Chambers, Wagener, and Weaver.[57] These thick films indicate a breakdown in the fcc structure with changes suggestive of bcc Fe.[69]

The 0.9-ML films show obvious peaks in the XPS angular anisotropy near 45° for growth at both 80 and 300 K. These peaks suggest significant second-layer growth. The peak anisotropy, maximum minus background, of the 0.9- and 1.6-ML films grown at 300 K are 26% and 25%, respectively, and neither shows a third-layer $\sim 0°$ peak. This suggests that the deposition of 1–2 ML of Fe at 300 K produces a fcc double layer. Also supporting of this proposition is an earlier report of second-layer growth after a deposition of only 0.1 ML of Fe.[62] In comparison, the 80-K grown 1.0- and 1.7-ML films have anisotropies of 13% and 22%. The 1.7-ML film has a weak peak in the angular anisotropy near 0°. These structures indicates that these Fe films consist of both single-layer and double-layer regions, with some three-layer regions for the 1.7-ML film.

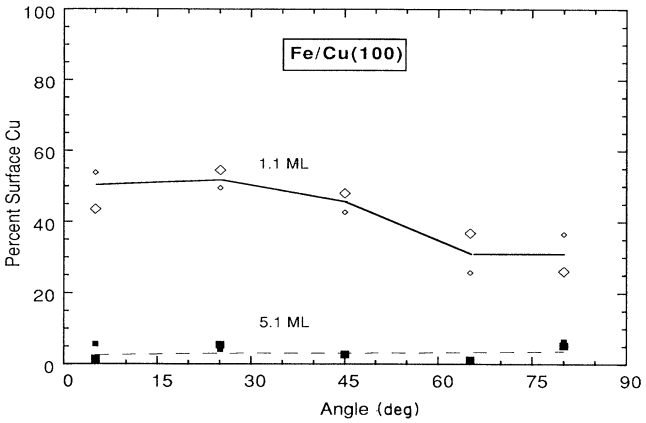

FIG. 14. The fraction of Cu in the surface for Fe deposited on Cu(100) measured using CO-titration technique for varying detection angle. Diamonds and squares are for 1.1- and 5.1-ML films grown at 300 K, respectively. Large and small symbols denote results for adsorption and desorption cycles. Results are consistent with early bilayer formation followed by nearly complete coverage of the Cu(100) by 5 ML.

The one- and two-layer structures of the nucleating film permit a simple interpretation of the XPS angular anisotropy. Consider a fcc(100) film consisting of a two-layer fraction x and a single-layer fraction y. The single-layer isotropic signal intensity is a constant A. The double-layer signal may be taken as the same constant A, for the top layer, plus an enhancement or anisotropy term B, for the underlayer. A good illustration of these angular anisotropies is in the layer-by-layer growth of Cu/Ni (100).[165] A simple analysis yields a convenient relationship between the measured anisotropy ζ and the double-layer fraction $z = x/(x+y)$,

$$\zeta(z) = \frac{zB}{z(A+B)+(1-z)A} . \tag{4}$$

A more useful expression, obtained from Eq. (4) by eliminating $B/(A+B)$, is

$$\zeta(z) = \frac{z\zeta(1)}{1+(z-1)\zeta(1)} . \tag{5}$$

$\zeta(1)$ is the anisotropy of a double layer, which is independent of the actual substrate coverage. In practice, $\zeta(1)$ is taken from a convenient film, such as a completed two-layer or double-layer film. The composition (x,y) of any other compound single and double-layer film can then be

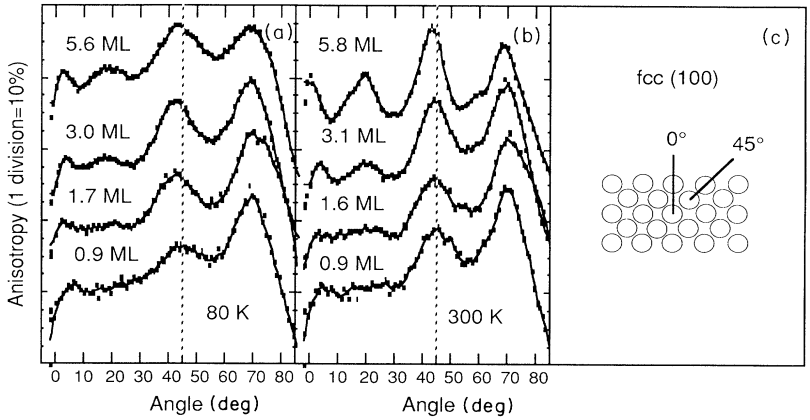

FIG. 15. XPS angular anisotropy for Fe films grown on Cu(100) at (a) 80 K and (b) 300 K using Fe $3p_{3/2}$ photoelectrons. Schematic diagram indicating directions of scattering enhancement for fcc(100) is shown in (c). Bilayer formation is evident for early growth. Small shifts for peaks at 0° and 45° (dashed line) show deviations from ideal fcc(100) growth. The rising intensity $>60°$ together with a sharp instrumental cutoff above 70° artificially enhances the 70° peak.

easily determined from the measured anisotropy of the film.[166]

As a calibration of Fe double-layer anisotropy $\zeta(1)$, we use the Fig. 15(b) data for 0.9- and 1.6-ML films grown at 300 K. These films have nearly identical 45° anisotropies (and double-layer fractions) of 26% and 25%. This allows us to estimate the double-layer concentrations for 0.9 and 1.7-ML films grown at 80 K as 43% and 82%, respectively. Using the 3.0-ML film grown at 300 K as a measure of third-layer 0° anisotropy, we can estimate that in the 1.7-ML film deposited at 80 K the three-layer fraction is roughly 40% of the film. Using these proportions, we can find the percentage of exposed substrate for 0.9- and 1.7-ML films grown at 80 K: 35% and 18±3%, respectively. This estimate compares reasonably well to the *average* of the adsorption and desorption CO-titration values of 30% and 10% Cu in the exposed surface. A similar analysis for the 0.9-ML film, which gave a high 54% Cu value, gives a similar forward-scattering estimate of 39%. Therefore, the deviations in the titration estimates are not reproduced in the forward-scattering results; however, the average results are in reasonable agreement. Finally, we can calculate the fraction of Cu in the exposed surface for the 0.34- and 0.51-ML Fe films grown at 80 K. The forward-scattering anisotropy gives estimates of 73% and 60% Cu in the exposed surface, which is about 10% above the average titration estimates.

To explain the disparity between the forward-scattering and CO-titration estimates, we must include substrate blocking and film instabilities. Blocking of the substrate Cu results in underestimates of substrate coverage for the CO-titration measurements as explained above. Blocking should be most important for the thinnest films and for the adsorption cycle, which is also where the CO-titration and forward-scattering estimates are most different. On the other hand, the CO-titration desorption measurements probably overestimate the substrate coverage of the as-grown films, because of changes in the film from annealing to 300 K with CO. Therefore, the true substrate coverage is probably intermediate between the CO-titration adsorption and desorption estimates, which agrees well with the forward-scattering predictions. In conclusion, if we plot the forward-scattering coverage estimates, we again find more Cu in the exposed surface than predicted by the downward funneling model and closer agreement with the Poisson model, Fig. 13(b).

Also, we compare these results with previously published CO-titration data.[62] Despite different substrate preparation and more grazing XPS detection angle (60° rather than 25°), the agreement is good with representative values of the fraction of Cu in the exposed surface as 46% Cu for 1 ML deposited at 300 K, 41% Cu for 0.4 ML deposited at 100 K, and 10% Cu for 1.4 ML deposited at 100 K.

RHEED oscillations for room-temperature growth of Fe/Cu(100) are shown in Fig. 16. Similar RHEED oscillations have been reported by several other groups.[67,128] The structure of the periodic oscillations naturally suggests three regions of growth defined by the thickness ranges: 0–4 ML, 4–10 ML, and >10 ML. During the initial film growth, the first intensity maximum is completely missing and the intensities for the second and third maxima are reduced. As shown by the titration and forward-scattering results, the missing oscillation can be understood as resulting from an apparent bilayer growth mode, when growth occurs by step propagation.[101,161,167] In contrast, RHEED oscillations measured for growth at 80 K (Ref. 161) and 450 K (not shown) have a strong first oscillation, which indicates a changing initial growth mode with substrate temperature. The peak denoted by 2 ML in Fig. 16 roughly indicates completion of the first two layers. The marked change for the fourth maximum indicates a drastic change in growth mode. Glatzel *et al.*[66] have suggested that the third and fourth layers also tend to nucleate as bilayers. Our data show that the second bilayer formation, if present, must be less prevalent than the first bilayer formation. Between thicknesses of 4 and 10 ML, the growth is characterized by slowly damping oscillations. This region is characterized by island coalescence followed by predominantly layer-by-layer growth. Above the 10 ML thickness, there is an abrupt decay in intensity and no oscillations. Forward scattering, reported by Chambers, Wagener, and Weaver,[57] shows a slow decay of structure in the XPS angular anisotropy above this thickness. The RHEED pattern itself shows dramatic changes. After deposition of

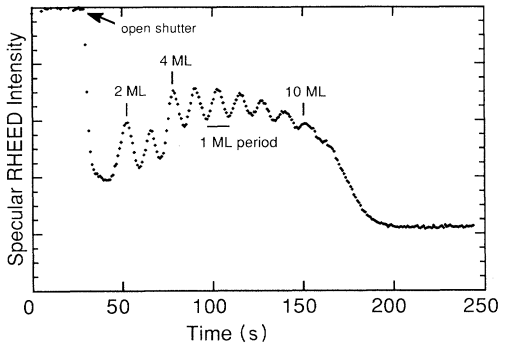

FIG. 16. RHEED oscillations for Fe grown on Cu(100) at 300 K. Measurements were made with channeltron detection of the specular spot intensity using 5-keV electrons having a grazing 2° incident angle. Numbers approximately indicate completed fcc layers; note missing first maximum. Initial bilayer growth is followed by near layer-by-layer growth. After deposition of 10 ML, a decay in the oscillations marks a changing crystalline phase.

12 ML, the off-center streaks symmetrically split into two with a subtended angle of $10.5\pm1.0°$. This splitting can be interpreted as the formation of bcc domains [see the general discussion for Cu(100) film growth].

The LEED patterns for Fe/Cu(100) are complex and have been studied by several groups. For Fe depositions up to ~3 ML, the LEED patterns of the films are predominantly (1×1) with narrow, fuzzy rings encircling the primary spots. These rings are most distinct for the 80-K grown films. The angle between the principal beam and ring is measured to be about 10% of the reciprocal vector. This spot profile indicates that the film surface is ordered with a characteristic length of about ten atomic spacings.[168] (Preliminary SPA-LEED measurements confirm these rings and indicate a characteristic distance between islands.[102]) Weak streaks also develop in the LEED patterns between adjacent spots for thicknesses above 2 ML. Some groups report a (4×1) LEED pattern for films near this thickness.[125,128] The LEED streaks sharpen to a (5×1) pattern for 4-ML-thick films, in agreement with several LEED studies.[66,67,128,131] For films 6 ML thick, we have observed a (2×1) pattern that has been reported as $p2mg(2\times1)$ (Ref. 16) or $p(2\times2)$-$p4g$ (Ref. 125) or simply a nonideal (2×1).[130] This pattern is interpreted by these authors[16,125] as a periodic displacement of the top Fe atoms from their pseudomorphic positions.

In addition to observation of the LEED patterns, we also estimated the Fe interlayer spacing. The spacing was determined by measuring the energies of the Bragg peak maxima in the specularly reflected beam. Simple kinematic LEED theory allows the interlayer spacing d to be determined from the slope of the Bragg peak energy versus the order number n^2.[169] Figure 17 shows data for clean Cu(100), a 3.7-ML Fe/Cu(100) grown at 80 K and a 5.9-ML Co/Cu(100) grown at 300 K. Also included is the kinematic prediction for Cu(100) using $d=1.805$ Å and an inner potential of 10 eV. The close agreement between the measured and predicted Cu energies above 200 eV shows that the multiple-scattering effects are relatively unimportant. From the ratio of the experimental slopes we estimate the Fe interlayer spacing to be 1.93 Å, this is expanded by 7% relative to the Cu lattice. The estimated Co interlayer spacing is 1.70 Å, contracted 6% with respect to the Cu. This surprising large Fe expansion is also substantiated by the forward-scattering results. Figure 15 shows the XPS angular anisotropies of 3.0 and 5.6-ML films grown at 80 K and a 5.8-ML film grown at 300 K. There is a shift in the 45° peak to ~43°, which corresponds to a ~7% expansion. A similar shift is also shown in the data of Chambers, Wagener, and Weaver for films grown at room temperature and thicker than ~8 ML.

Certainly these interlayer spacings must be considered approximate given the simplicity of the analysis, but they do serve as a guideline. More sophisticated approaches also report substantial changes in lattice spacing for different growth temperatures and thicknesses. Fe films grown at 423–473 K are reported to show little or no lattice change compared to the Cu.[13,17] However, films grown at room temperature show substantial relaxations compared to Cu, and we list those reports here. Clarke *et al.*[124] found expansions increasing linearly with thickness and reaching a maximum interlayer expansion of 4% for the top layer and 6% for the bulk. Lu *et al.*[127] found inconsistent model results for 1, 2, and 3 ML of Fe, while modeling for a 12-ML film gave a 4% first layer expansion and a bulk 2% contraction. An 8-ML film, studied by Hezaveh *et al.*[123] using Bragg peak fitting, showed little or no change in spacing, but contamination may be a contributing factor. Landskron *et al.*[67] included a reconstructed surface in their analysis of a 6-ML film and found evidence of a 4% top-layer expansion with an alternating 0.14-Å lateral displacement.

The reconstructed LEED patterns and the small

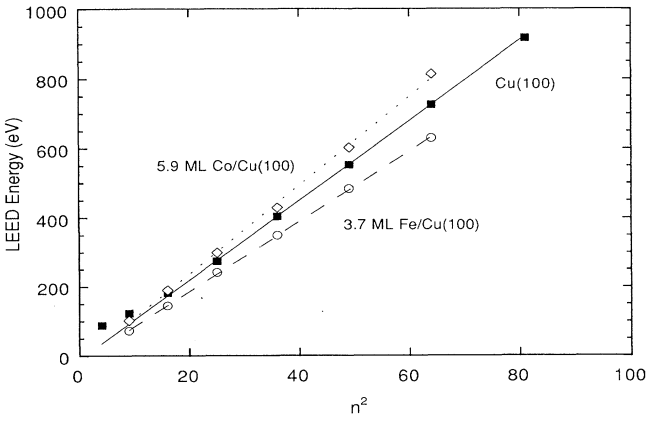

FIG. 17. LEED energy of Bragg maximum vs order number squared. Solid curve indicates kinematic prediction for Cu(100) that agrees well with solid square Cu data points. Dashed and dotted lines are linear fits to the data for energies over 200 eV. Slopes are used to estimate interplanar separations.

changes in the XPS angular anisotropies (Fig. 15) pose a question: can reconstructions of the surface layer account for both observations? First, we must establish the origin of the (4×1) and (5×1) LEED patterns. A model for the (5×1) pattern, similar to the (2×1) pattern, has been proposed that amounts to periodic displacements of the top atoms.[16] Another model suggests that there is a preferential formation of terraces with four and five atomic widths.[170] In addition, a periodic displacement is also necessary, such as a glide plane symmetry as in the first model. The driving force for either of these models is not clear. In fact, both models appear to do little to decrease the surface free energy of the Fe, which is an important factor given the inherent strain and relatively high surface free energy of the open (100) fcc Fe surface. It therefore seems appropriate to examine two alternate models, which have not been suggested in the literature. Both of these models, or close derivatives of them, are believed to describe the surface reconstructions of (100) crystal faces for the fcc metals Ir, Pt, and Au. Consideration of these models seems particularly appropriate since Ir displays a (5×1) pattern and the Pt and Au have more complicated patterns that are related to the (5×1) pattern. For an excellent discussion of these reconstructions see Van Hove *et al.*[171] The first model proposes a hexagonal top layer that maintains a fivefold periodicity with the square (100) lattice [see Fig. 18(a)]. The unit cell of the surface contains six atoms, which should be compared to five in the reconstructed layers. This 20% increase in density is accomplished with only a 3.27% contraction along the fivefold direction. This hexagonal surface layer can be viewed as a fcc (111) close-packed layer, or equivalently, a weakly sheared bcc (110). The (111) fcc will have a much lower surface free energy than the (100) fcc face. In addition the small 1.2% expansion from the fcc Fe bulk lattice is replaced by 2.1% compression. The second reconstruction is described as the shifted-rows model [see Fig. 18(b)]. Two of every five rows are shifted half a lattice spacing along the in-plane (010) direction. This shift leaves 60% of the atom positions unchanged. A unit cell contains five atoms with separated rows of either three, four, or five atoms (which are not all shown in Fig. 18). The effective area of the reconstructed clusters is reduced by 5.4%, which again serves to reduce the surface free energy. The advantage of this model lies in simple generalizations to the (4×1) and (2×1) LEED patterns.

Returning to the XPS angular anisotropy data of Fig. 15, we can now begin to evaluate these models. The strong although slightly broadened 45° peak indicates the film is predominantly fcc. A 3.7-ML film grown at 80 K and warmed to 375 K displayed a beautiful (5×1) LEED pattern. However, there was no significant change in the XPS angular anisotropy peak at 45° for this film compared to the angular anisotropies obtained from films that displayed no clear reconstruction. Apparently the surface reconstruction is only a small perturbation to this forward-scattering peak. We can expect that the normal emission forward-scattering peak will be more sensitive to the top reconstruction, since it arises from forward scattering of next-nearest layers. Indeed the weakened intensity in the XPS angular anisotropy near 0° can be viewed as evidence of the reconstruction. Comparing the two models, the shifted-rows model leaves more than half of the top layer unchanged. We would therefore expect that at least 50% of the 0° intensity in the angular anisotropy would remain unaltered according to this model, but this is not consistent with Fig. 15. The higher-order coincidence of the hexagonal reconstruction removes the polar symmetry for a reconstructed domain of the film, although on average the symmetry remains. The lower local symmetry should alter the 0° forward-scattering peak from the dominant first and third layers. Therefore, this model appears to be more consistent with the data. However, detailed calculations are necessary to discern the precise XPS angular anisotropy for such a complex structure. The 0° peak in the XPS angular anisotropy appears to return for a 5.8-ML growth at 300 K. This changing structure in the angular anisotropy is not strictly due to growing vertical disorder, which may be expected to simply increase with film thickness. Although these data are not definitive, we believe these models are consistent with our observations and worthy of further study.

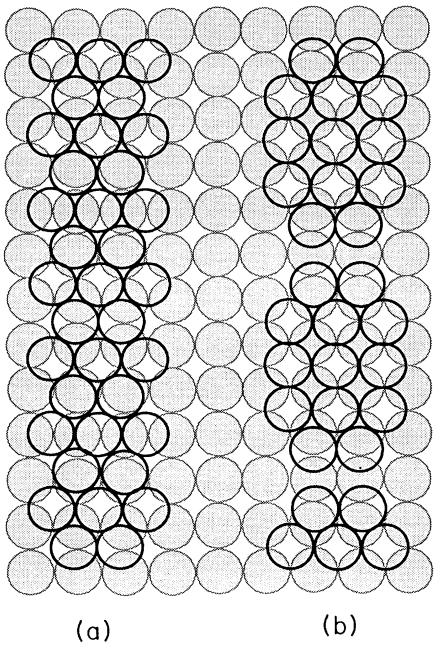

FIG. 18. Schematic illustration of basic 5×1 surface reconstructions of fcc(100) Ir, Pt, and Au. Reconstructed surface atoms are shown by open bold circles. Second layer atoms in fcc(100) lattice positions are indicated by shaded circles. (a) depicts a domain of a hexagonal surface layer. (b) shows a possible missing row reconstruction having a five-row unit cell. Different coincidences of these basic structures are also possible.

B. Co/Cu(100)

Co films of varying thickness were grown at Cu substrate temperatures of 80 K and 300 K. The system

structure was characterized using LEED, RHEED, forward scattering and CO-titration.

CO-titration measurements of the fraction of Cu in the surface were made for films up to 6 ML thick. Figure 19(a) shows these data for the absorption and desorption cycles. There is generally an increase in the fraction of Cu in the exposed surface after warming with adsorbed CO much like the Fe. Like Fe/Cu(100), the increase in the fraction of Cu in the surface for the desorption cycle is mainly attributed to undetermined instabilities in the film. The variations in measured Cu for a given deposition of Co can again be correlated with changes in the substrate (Table IV). Deposition of 0.85 ML of Co at 80 K gave 43% Cu in the exposed surface (on the third day of experiments). Another 0.85 ML Co film, deposited at 80 K on a 20 ML Cu buffer layer, which was grown at 600 K, showed a lower value of 7% Cu in the surface. An intermediate value of 20% Cu in the surface was measured for a 0.85 ML film prepared three weeks later. Finally, a low value of 14% Cu in the surface was obtained for another 0.85 ML film, which was deposited at 80 K on a surface that was sputtered but not annealed. A 0.51 ML film grown at 80 K gave 31% Cu in the surface; indicating partial blocking of the substrate by the Co ($0.31+0.51=0.82$ not 1.0). Like Fe/Cu(100), this substrate blocking effect appears especially important for high-defect-density substrates. Overall these results are analogous to those obtained for similar Fe films grown with equivalent preparations (see Table IV).

The fraction of Cu in the exposed surface depends upon the Co film thickness (Fig. 19) much like Fe [see Fig. 13(a)]. In particular, films grown at 300 K show similar titration results for Co and Fe—as the nearly identical surface mobilities would imply (Table V). There is an exponential decrease in the fraction of Cu in the exposed surface that indicates near-complete substrate coverage ($<5\%$) around 3 and 5 ML of Co, for growth temperatures of 80 and 300 K, respectively. This ~ 1.5-ML offset between coverages appears to continue down to ~ 1 ML of deposited Co.

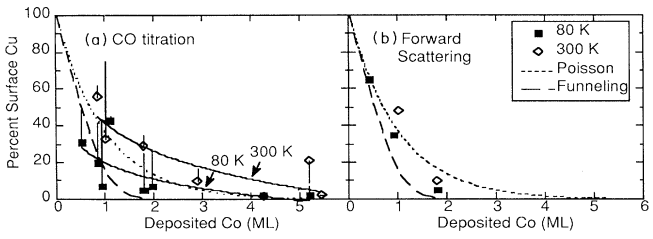

FIG. 19. The fraction of Cu in the surface for Co deposited on Cu(100) at 80 and 300 K. (a) shows Cu values determined by CO-titration technique using a 25° detection angle. (b) shows exposed Cu substrate values determined by XPS angular anisotropies. Solid squares and open diamonds indicate as-grown measurements for growth temperatures of 80 and 300 K. Error bars indicate changes for desorption titration cycle. Solid curves show exponential fits to the as-grown data. Dashed and dotted curves show the fraction of Cu in the surface for predictions based upon downward funneling and Poisson random deposition models.

To investigate the magnitude of surface segregation at higher growth temperatures, two films were grown at 450 K. These 1.9- and a 4.3-ML films gave average exposed copper values of 75% and 55%, respectively, which compares to exposed copper values of 29% and 17% for equivalent depositions at 300 K.

Angle-dependent CO-titration measurements were made for 4.3-ML films grown at 80, 300, and 450 K. Figure 20 shows that the 80- and 300-K grown films are quite similar in terms of the distribution of Cu at the exposed surface. However, the 450-K grown film show substantially more Cu in the surface, about 35% and 40%, than equivalent depositions at 300 and 80 K. Using the model previously proposed for the (111) films, we can estimate the distribution of Cu in the surface. The solid curves in Fig. 20 show fits to the data. The data display a slightly concave curvature unlike the fits that are convex. This concave curvature in the data may be accounted for by the likely formation of (111) facets on the cluster sides, which would reduce the Cu $2p_{3/2}$ signal attenuation for angles less than 45°. These fits suggest that increasing growth temperature increases the substrate exposure slowly, but increases the copper segregation abruptly. The segregated Cu increases from monolayer fractions of $\sim 0\%$ at 80 K, to 7% at 300 K, and to 40% at 450 K. This is consistent with Kerr effect, hydrogen titration, and angle-resolved ultraviolet photoemission spectroscopy studies that found a temperature threshold of 375 K for copper surface segregation in the Co/Cu(100) system.[58,156]

XPS angular anisotropies for films of Co/Cu(100) grown at 80 and 300 K are shown in Figs. 21(a) and 21(b).

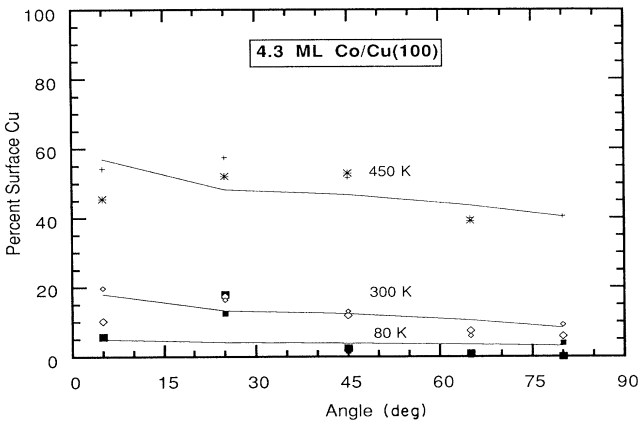

FIG. 20. Fraction of Cu in the surface for Co on Cu(100) measured using CO-titration technique for varying detection angle. A 4.3-ML film of Co was deposited at 80, 300, and 450 K. Large and small symbols denote values obtained from adsorption and desorption cycles, respectively. Curves show fits to the data using a simple model allowing for visible substrate Cu and segregated Cu (see text). Growth at 80 K shows almost no Cu in the surface. The data for the film grown at 300 K are fit with 7% segregated Cu and 10% exposed substrate Cu. The data for the film grown at 450 K are fit using 40% segregated Cu and 17% exposed substrate Cu.

The evolution of the film structure, as shown by the angular anisotropy, is quite similar for the two growth temperatures. Even at 80 K, the first layer shows substantial second-layer occupation indicated in the angular anisotropy by a strong 45° peak and no 0° peak. The 0° peak develops only after a deposition of 3 ML, showing that the first two layers are mostly completed before the third layer begins. Deposition of 5.2 ML at 80 and 300 K produces films that are well ordered and virtually identical in angular anisotropies. Comparing the angular anisotropies of the 0.9- and 1.8-ML depositions at 300 K yields similar 45° anisotropies of 36% and 39%. Recall that identical 45° anisotropies were also found for 0.9- and 1.6-ML films of Fe/Cu(100). We conclude that the apparent bilayer agglomeration is roughly comparable for Co and Fe films grown at 80 and 300 K. We can estimate the substrate coverage by taking the 39% anisotropy as a measure of bilayer anisotropy. Deposition of 0.5, 0.9, and 1.8 ML at 80 K resulted in a 68%, 31%, and 0% fraction of Cu in the surface, respectively. A 1.0-ML film deposited at 300 K had 45% Cu in the surface. These values are shown in Fig. 19(b). We again find slower substrate coverage than predicted by the downward funneling model. Using our bilayer model with angular anisotropies obtained by a different group[70] gives the fraction of Cu at the surface as 55% for 0.7 ML and 32% for 1.1 ML of Co deposited at 300 K. These independent data agree with our Fig. 19. We also tested the role of surface defects and annealing on the initial Co film growth. We measured XPS angular anisotropies for 0.85-ML films grown at 80 K on a sputtered but unannealed substrate and on a properly prepared substrate with annealing to 300 K after Co deposition. The fraction of Cu in the surface was 30% for the sputtered substrate and 50% for the annealed film. The first result shows that a higher density of surface defects do not significantly alter the initial substrate coverage for growth at 80 K and that variations in titration results are predominantly due to Co blocking substrate Cu atoms from CO adsorption. The result for the film annealed to 300 K is very close to the value obtained for a film grown at 300 K, indicating that growing at 300 K or annealing to 300 K produces similar films, like Fe/Cu(100).

The initial Co growth may also be reflected in the room-temperature RHEED oscillations shown in Fig. 22. The first peak is much weaker than the subsequent maximum. The regular oscillations indicate predominantly layer-by-layer growth for 2–10 ML. A similar behavior is displayed for Fe/Cu(100), where the first maximum appears entirely damped at 300 K (Fig. 16). Similar RHEED oscillations have also been reported for Co grown on Cu(100) at room temperature, while film growth at 450 K showed no damping of the first maximum,[58] like Fe. Temperature-dependent He scattering measurements show a very similar behavior;[154] a pronounced first maximum for growth at 418 K that decays with decreasing temperature until the first maximum is missing for growth at 270 K. In contrast, Co (Ref. 172) and Fe (Ref. 161) films grown at 80 K have regular RHEED oscillations and the first maximum does not appear damped. Therefore, the dampening of the first RHEED maximum seems to display an interesting reentrant type of behavior for Co and Fe films grown on Cu(100). This behavior is reminiscent of Pt/Pt(111).[100,101]

Increasing the growth temperature from 300 to 450 K has been shown to strongly promote Cu surface segregation. The consequences of the surface segregated layer are shown in Fig. 23. The XPS angular anisotropy for 2-ML films grown at 80, 300, and 450 K using Co $3p_{3/2}$ (1425 eV) are compared to the XPS angular anisotropy of clean Cu(100) using Cu $3p_{3/2}$ (1409 eV). The 80- and 300-K grown films show a small shift in the primary peak to 47°. The 450-K grown film and Cu(100) substrate show no such shift with a peak at 45°. In addition, the 450-K grown film shows a weak 0° maximum. The angular anisotropy of the 450-K grown film is nearly identical

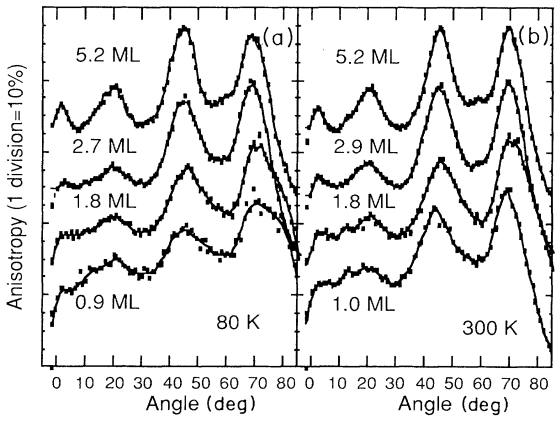

FIG. 21. XPS angular anisotropy for Co films grown on Cu(100) at (a) 80 K and (b) 300 K using Co $3p_{3/2}$ photoelectrons. Bilayer formation is evident for early growth. Growth at 80 K produces very similar structure to growth at 300 K. The rising intensity > 60° together with a sharp instrumental cutoff above 70° artificially enhances the 70° peak.

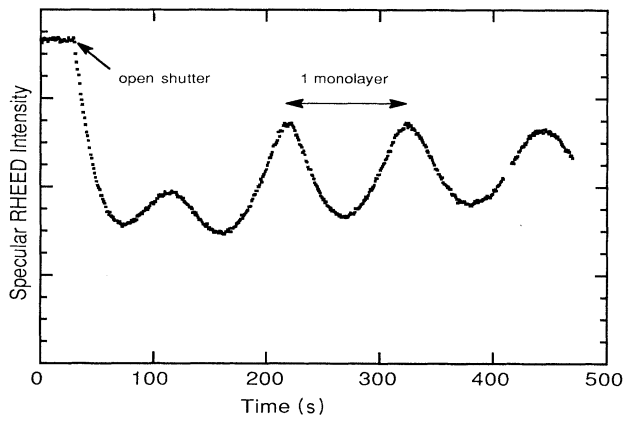

FIG. 22. RHEED oscillations for Co grown on Cu(100) at 300 K. Conditions were the same as in Fig. 16. The first maximum is reduced, similar to Fe/Cu(100), with subsequent oscillations indicating near layer-by-layer growth.

to that of the 2.9-ML Co film grown at 300 K [Fig. 21(b)], which indicates that the Co remains in the top three layers. CO titration estimates that the exposed surface of the 450-K grown film is 75% Cu. These data suggest that deposition of 2 ML of Co at 450 K results in a sandwich structure, where the 2 ML of Co are nearly covered by Cu. These data support the earlier interpretation that for 450-K growth the Cu tends to segregate to the surface rather than alloy with the Co or have the Co simply agglomerate. The bulk immiscibility of Co and Cu (Ref. 173) combined with the lower Cu surface free energy[3] is the thermodynamic driving force for this sandwich structure. The films grown at 80 and 300 K show a shift of the 45° fcc peak to 47° in the XPS angular anisotropies. This shift is equivalent to a 7% contraction of the Co lattice relative to the intraplane Cu spacing. This agrees very well with the Bragg LEED analysis that gave a 6% contraction (Fig. 18) for a 300-K grown film. Also, a detailed LEED *I-V* analysis for a 8-ML Co film grown at room temperature gave a 6% first layer contraction and bulk 3% contraction.[20] Helium-atom scattering found a 4% contraction for Co films grown at 420 K, but no relaxation after coating with 5 ML of Cu.[155] Our observations suggest the more dramatic result that the large Co relaxation is relieved by the Cu layer ($\sim$1 ML) that segregates at 450 K. Comparable, extensive relaxation effects have recently been reported for Cu capping of Fe/Cu(100).[129] Further evidence for this conclusion is given by LEED *I-V* results of Schneider *et al.*[174] for growth at 450 K, which also show no change in interlayer spacing relative to Cu for 2 ML of Co. Although, 5 ML of Co grown at 450 K has a 5% interlayer contraction, in reasonable agreement with our films grown at 300 K. Apparently the segregated Cu is less effective in reducing the Co relaxation as the film thickness increases.

C. Discussion

Results from CO-titration and forward-scattering measurements both indicate a predisposition for what appears to be an initial bilayer growth of Fe/Cu(100) and Co/Cu(100) at room temperature. We find less than 10% of a ML of Cu surface segregated at 300 K, which agrees with the previously reported thresholds for significant Cu surface segregation of 375 K (Ref. 58) and 360 K (Ref. 62) for Co/Cu(100) and Fe/Cu(100), respectively. However, 2- and 4.3-ML films of Co/Cu(100) grown at 450 K result in a segregated Cu layer of about 0.5 ML. For comparison, we note that a previous study found that a 5.2-ML Fe film grown at 425 K showed 0.46 ML of Cu at the surface[62] (however, no distinction was made between substrate Cu and segregated Cu in this study).

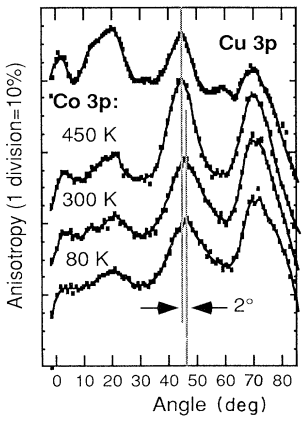

FIG. 23. XPS angular anisotropy for 2-ML Co films grown on Cu(100) at 80, 300 and 450 K using Co $3p_{3/2}$ photoelectrons. Also shown is XPS angular anisotropy for clean substrate using Cu $3p_{3/2}$. A small $\sim$2° shift in the 45° peak indicates a $\sim$7% contraction of the Co interlayer spacing for films grown at 80 and 300 K. No relaxation is observed for the film grown at 450 K.

As discussed above, our CO-titration and XPS angular anisotropy data suggest that the nucleating Fe and Co films on Cu(100) at 300 K form regions with large bilayer areas. However, recent STM studies[71,131,133] suggest that this model may be too simple. Chambliss, Wilson, and Chiang[131] argue that simple bilayers are not nucleated but instead Fe adatoms displace substrate Cu atoms in the surface. Brodde and Neddermeyer[133] observe some two-layer growth and report that the Fe adatoms reactively roughen the Cu steps. Schmid and Kirschner[71] report that a second Co layer nucleates well before the first Co layer is completed. Overall, there are qualitative and quantitative discrepancies between all these studies that are not easily explained. We believe that our own experiments which are element specific are self-consistent. In contrast, there are inherent difficulties in discriminating between Fe, Co, and Cu atoms using STM and this may complicate the interpretation. Tentatively, we retain our picture of early Fe and Co bilayer formation. Although it is unclear how these bilayers form, the simplicity of this picture is attractive. It well may be that this picture is oversimplified and we do not yet completely understand the complexity of these systems.

Growth at 80 K inhibits surface mobility and reduces the tendencies toward bilayer growth. Our analysis of the XPS angular anisotropies suggests that the substrate coverage is less than predicted by the "downward funneling" model and closer to Poisson statistics. CO-titration results generally support this interpretation, if we allow for blocking of the substrate Cu by the Fe or Co. The blocking is seen to be particularly important for low coverages at low growth temperatures (i.e., small clusters) and high-defect-density surfaces where cluster perimeters are expected to be maximal. An explanation for the blocking effect can be found in the report of increased CO-saturation density for low coverages of Co on Cu(100) ($\sim$30% increase in CO from 1 to 0.3 ML).[175] We postulate that this higher CO packing density on the Co results in partial blocking of the adjoining, weak binding Cu(100) sites.

The measured Cu substrate coverage for Fe and Co depositions at 80 K (Figs. 13 and 19) should not be accepted as evidence for *no* adatom mobility, since the rings observed by LEED indicate enough mobility to nucleate islands with an average separation of about ten atoms. Moreover, random deposition with zero mobility results in overhangs and unstable configurations that are unphysical. However, the substrate coverage appears less extensive than predicted by the downward funneling

model. The Monte Carlo simulations of Young and Schubert[176] predict substrate coverage less than random deposition but more than downward funneling. This can be accounted for by permitting an adatom to lie in "interstitial" positions, supported by only three underlying condensed atoms—a questionable arrangement for flat substrates, but more reasonable if we include substrate steps. Nevertheless, these Monte Carlo simulations report changes in substrate coverage $\leq 10\%$ even with two hops. This results in coverages intermediate between random deposition on a simple cubic lattice and downward funneling and within the accuracy of our measurements. Therefore, low mobility may alter substrate coverage only weakly.[177] This crucial distinction between no mobility and low mobility is demonstrated by the presence of RHEED oscillations even at 80 K, well below temperatures where thermal diffusion is expected (Table V and see Ref. 16). Although it has been shown that there are no RHEED oscillation for purely random deposition with no mobility, relaxing the constraints to allow for random deposition at (100) fourfold hollow sites can produce oscillations while maintaining random statistics for the first layer.[160,164]

Better agreement between measured substrate coverage and theory requires a more realistic description, such as a downward funneling model that considers (1) adatoms that have low but nonzero transient mobility or (2) deposition on a nonideal surface that has steps. If the adatoms have a tendency to cluster, the probability increases for a second layer atom to be fully supported by four first-layer atoms. This will effectively increase the amount of exposed copper from the funneling model estimate toward the Poisson model estimate. Alternatively, consider the surface of a stepped fcc (100) Cu substrate that can be described as an initially flat surface upon which an additional X monolayers of Cu atoms have been randomly deposited. If $X<1$, the Cu surface consists of two atomic levels, $(1-X)$ ML in the first level and X ML in a second level, which is one atom higher. For X near 0 or 1, the number of vacancies will be small and steps will be large. If we now deposit Fe, the downward funneling prediction of the Fe-layer growth and the Cu-substrate coverage will be effectively offset by X ML. This offset means that a surface with 50% ($X=0.5$) of the atoms in a second layer requires 2.0 ML of deposited material to obtain a substrate coverage of 96.7% rather than 1.5 ML of deposited material for a flat substrate.[164] Even more deposited material would be required for $0.0<X<0.5$. Of course, this estimate is too crude and coverage also depends upon the substrate step height and distribution, which we have taken to be random. Nevertheless, this simple illustration shows that substrate steps can alter substrate coverage significantly and a more accurate picture requires careful consideration of substrate steps. It also provides a guideline showing that substrate steps should reduce the rate of substrate coverage with film deposition. Therefore, the slow substrate coverage relative to the downward funneling model observed in Fig. 13 and 19 might be attributable simply to finite mobility or substrate steps. This also shows that the CO-titration estimates for high-defect-density substrates that gave near-complete coverage after deposition of only 1.0 ML of Fe (Table IV) can again be attributed to blocking of CO adsorption, rather than genuine coverage. To investigate these issues further, we are currently studying the step density and surface morphology of our substrates using SPA-LEED.

The reentrant behavior of the first RHEED maximum with growth temperature is an important clue to the Fe and Co on Cu(100) growth dynamics. The minimum in the first intensity maximum signals a transition between growth modes driven by changing adatom mobility. The slow substrate coverage dependence shown above suggests a low-temperature growth mode distinguished by transient, low mobility. The resulting films have a tendency to form small islands as shown by LEED. The intermediate (room temperature) growth mode is initiated by what appears to be double-layer growth, which becomes largely layer by layer after substrate coverage. The higher temperature [450 K for Co/Cu(100)] growth appears aided by surface segregation of the Cu, which acts to reduce the surface free energy and promotes a more complicated layer-by-layer growth. This phenomenon has been previously suggested for Co/Cu(100) (Ref. 58) as well as for growth of Rh/Ag(100) (Ref. 163) and Fe/Au(100).[178] The resulting film has a reduced growth front, as indicated by better RHEED oscillations.[58] Finally we note that the reentrant RHEED first maximum is reminiscent of recent work by Kunkel and co-workers[100,101] of Pt/Pt(111) that showed no oscillation in He-atom scattering intensity at an intermediate temperature (424 K), but regular oscillations at 275 and 621 K. Kunkel and co-workers speculate that this transition is evidence of changing growth dynamics. The low- and high-temperature depositions correspond to two-dimensional growth while the intermediate temperature deposition is three-dimensional growth. The determining factor is the barrier for diffusion over descending steps. At high temperature, adatoms can hop over the barrier and at low temperature the barrier is reduced by the steps being jagged. At intermediate temperatures the steps are smooth and adatoms cannot hop over the barrier. A related picture could be envisioned for the early growth of Fe and Co on Cu(100). The controlling elements are the rate of surface diffusion and surface free-energy minimization. The intermediate growth temperature region corresponds to temperatures high enough to facilitate bilayer formation but not high enough to activate substantial Cu surface segregation.

The decay of the Fe/Cu(100) specular beam RHEED oscillations (Fig. 16) marks the departure from the fcc phase after 10 ML. Simultaneously we observe symmetric splitting in the RHEED spots off the [110] azimuth. Similar decays in the oscillations have been recently reported in 3 keV [100] RHEED oscillations between 12 and 15 ML with streaks developing along the $\langle 110 \rangle$ directions in both RHEED and LEED.[128] The forward scattering results of Chambers and co-workers[57,60] also suggest a developing bcc phase with the [100] direction near parallel to the surface normal. Our observations are largely consistent with these results but indicate that the growing bcc [100] interface plane is not

strictly coincident with the fcc [100] interface plane. This is reasonable to expect because the Fe fcc(100)/bcc(100) lattice mismatch of 25% is very unfavorable and there is no known simple orientational relationship.[77] Previous TEM studies[74] observed the formation of bulk misfit dislocations for Fe film thicknesses more than 20 Å. The Burgers vector of these dislocations were of the type $\frac{1}{2}\langle 110\rangle$, and were inclined at 45° to the film (100) surface. It is believed that the propagation of the dislocations precipitates the fcc-bcc phase transition.[75,106] We suggest that the splitting of the RHEED spots are indicative of the different domains of bcc Fe that result from this transformation. These domains appear rotated symmetrically by $10.5\pm1.0°$ with respect to the [110] azimuth.

V. GROWTH OF Fe AND Co ON Cu(110)

The structural and magnetic properties of Fe and Co films on Cu(110) has received little attention. Electrodeposited films of Fe/Cu(110) were studied using electron diffraction and electron spin resonance.[179] Vacuum evaporated monolayer Fe films were examined with LEED (Refs. 10 and 180) and thick Fe films were studied using TEM.[77] The structure of Co/Cu(110) was examined with SEXAFS.[88,89]

A. Fe/Cu(110)

Figure 24 shows the fraction of Cu in the exposed surface for Fe/Cu(110) measured by CO titration with growth temperatures of 80 and 300 K. In comparison to results obtained for Cu(111) (Fig. 2) and Cu(100) [Fig. 13(a)], we see that the Fe films grown at 300 K have substantially more Cu in the surface for the Cu(110) substrate. This large fraction of Cu in the surface persists

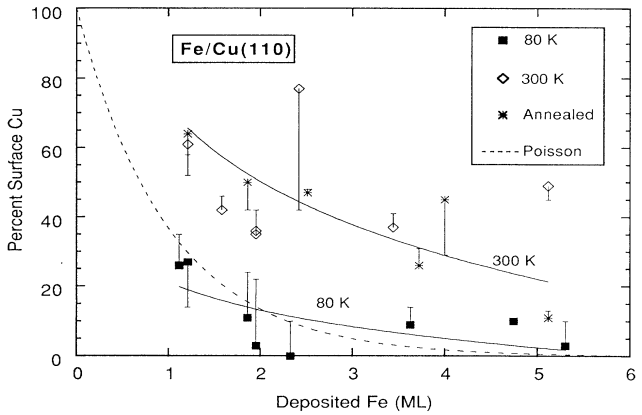

FIG. 24. The fraction of Cu in the surface for Fe deposited on Cu(110). Coverage is determined by CO-titration technique using a 25° detection angle. Solid squares and open diamonds indicate Cu values obtained for adsorption measurements with growth temperatures of 80 and 300 K, respectively. Stars indicate Cu values obtained for films grown at 80 K and annealed to 300 K before titration. Error bars indicate Cu values obtained for the desorption cycle. Solid curves show exponential fits to the as-grown data. The dotted curve shows the fraction of Cu in the surface according to the Poisson model.

even for a 9.4-ML deposition (not shown), which still had 6% Cu at the surface. The Fe films grown on Cu(110) at 80 K show very similar results to Fe/Cu(111) and the adsorption titration cycle for Fe/Cu(100). Briefly annealing the 80-K grown films to 300 K produces films with Cu values comparable to growth at 300 K, within 10%. This results indicates that growth at 300 K and annealing to 300 K produces films with similar fractions of Cu in the surface.

XPS angular anisotropy curves for Fe/Cu(110) are shown in Fig. 25. The two preparation temperatures produce very different angular anisotropies. The lack of structure in the angular anisotropy for the 1.-ML film grown at 80 K indicates the Fe must remain in the top one or two layers. The angular anisotropy of the 2.4-ML Fe film grown at 80 K shows slightly increased intensity near 0° and 45°. Even the 3.6-ML film shows only weak peaks in the angular anisotropy. These anisotropy peaks increase for the 5.1-ML film, but remain broad. In contrast, the 1.0-ML film grown at 300 K already shows strong peaks in the angular anisotropy at 0° and 45°; this requires that a substantial fraction of the Fe atoms reside in the third or deeper layer. Thicker films grown at 300 K display slowly sharpening peaks in their angular anisotropies. In general, the XPS angular anisotropies of Fig. 25 are representative of a distorted fcc(110) structure. The thinner films show a shift in the normal and central peaks out to larger angle indicating deviation from ideal fcc stacking. This distortion is equivalent to a lateral shift between the first and third layers of around 5% along the furrowed $[1\bar{1}0]$ direction. Note that no peak is observed in the angular anisotropy corresponding to the symmetric -5% shift. A small perpendicular compression would reduce this apparent shift. LEED *I-V* analysis found that an 11-ML Fe film grown at 300 K had a compression of $\sim 7.8\%$ between the first two layers, but the known faceting in the film makes the reliability of this estimate uncertain.[10] Annealing the 80-K films to 300 K produces films with angular anisotropies nearly identical to the 300-K grown films. This is consistent with the similarity observed in the CO-titration results discussed above (Fig. 24).

LEED patterns for the 80-K grown films are (1×1). A 1-ML Fe film has LEED that have sharp centers and a faint, yet defined width of about $\frac{1}{5}$ the nearest-neighbor separation. Thicker films also have (1×1) LEED patterns, but the spot intensity slowly decreases while the background increases more slowly. After deposition of 6 ML, the LEED spots of the films are barely visible. LEED patterns for films grown at 300 K show streaks along the $[1\bar{1}0]$ direction, which is parallel to the surface furrows. These streaks appear in the LEED for just 1-ML-thick films. The LEED pattern for 2-ML-thick films is (1×2). This pattern weakens but persists for films up to ~ 4 ML thick. Thicker films have LEED patterns that continue to show strong streaks, which indicate a $\{111\}$ faceted surface. Similar observations, including strong faceting up to 20 ML, have recently been reported by Tian, Jona, and Marcus.[10]

A (1×2) LEED pattern has also been observed for the fcc(110) surfaces of Ir, Pt, and Au. Among the many

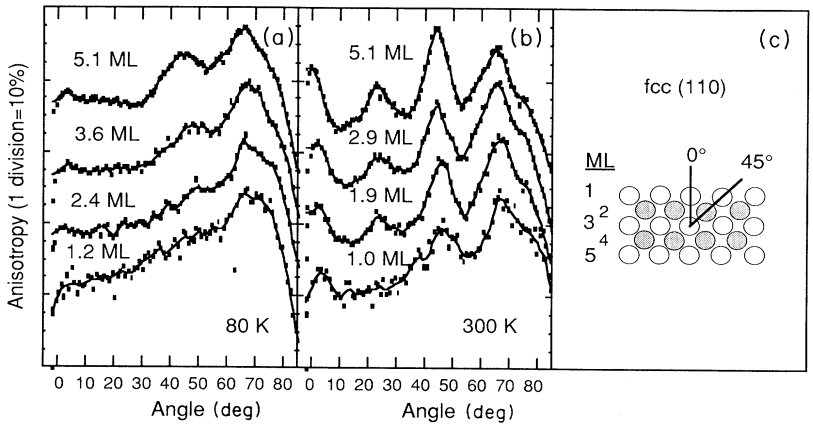

FIG. 25. XPS angular anisotropy for Fe films grown on Cu(110) at (a) 80 K and (b) 300 K using Fe $3p_{3/2}$ photoelectrons. (c) demonstrates that no scattering enhancements occur for the first two fcc(110) layers. The shaded atoms lie below the plane of the page. Growth at 80 K appears to produce flat films, while growth at 300 K is complex.

possible models for the surface reconstruction, the missing row model is generally preferred.[160] A similar model can explain the 2-ML Fe/Cu(110) result. The driving force for the reconstruction could be to minimize the Fe surface free energy through Cu surface segregation and/or the formation of closed packed (111) planes along the row sides. Figure 24 shows ~50% of the surface is Cu for deposition of 2 ML of Fe. However, this value should be viewed with caution since the effect of the large surface corrugation upon the CO adsorption geometry and titration results is unclear.

B. Co/Cu(110)

CO-titration results for Co films grown at 80 and 300 K on Cu(110) are shown in Fig. 26. The results are very similar to Fe/Cu(110) (Fig. 24). The 80-K grown films show a quickly declining fraction of Cu in the surface. The 300-K films display substantially more Cu in the surface. Even after 5 ML of deposited Co, the surface is still 20% Cu. A 2-ML film grown at 80 K and annealed to 300 K gave values of 37% and 51%, which are near the 300-K values. Like Fe/Cu(110), the decrease in the fraction of Cu in the exposed surface is approximated by an exponential decay with deposited Co (solid curves, Fig. 26).

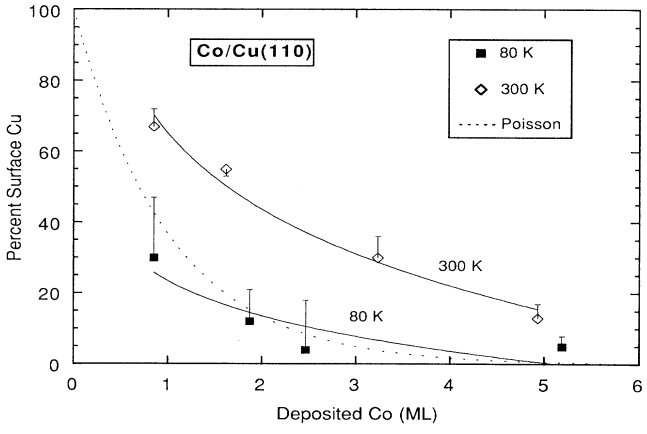

FIG. 26. The fraction on Cu in the surface for Fe deposited on Cu(110). Coverage is determined by CO-titration technique using a 25° detection angle. Solid squares and open diamonds indicate Cu values obtained for adsorption measurements with growth temperatures of 80 and 300 K, respectively. Annealing films grown at 80–300 K produces results similar to films grown at 300 K (not shown). Error bars indicate Cu values obtained for the desorption cycle. Solid curves show exponential fits to the as-grown data. The dotted curve shows the fraction of Cu in the surface according to the Poisson model.

XPS angular anisotropies of Co $3p_{3/2}$ for Co/Cu(110) are shown in Fig. 27. The 80-K grown films show clear 0° and 45° peaks in the angular anisotropies after deposition of about 2 ML. The 0.8-ML film grown at 80 K displays structures in the angular anisotropy that are inconsistent with fcc(110) layers, but there are indications that the data are unreliable. The angular anisotropy for Co $2p_{3/2}$ measured from the same 0.8-ML film shows no peaks. Also, no consistent peaks were observed in the angular anisotropies for Co $3p_{3/2}$ and Co $2p_{3/2}$ of a 1.7-ML film. Therefore, the XPS angular anisotropies for 1- and 2-ML films grown at 80 K suggest flat layer growth, yet must be considered inconclusive. For films from 5 to 20 ML thick grown at 80-K film, the structure in the angular anisotro-

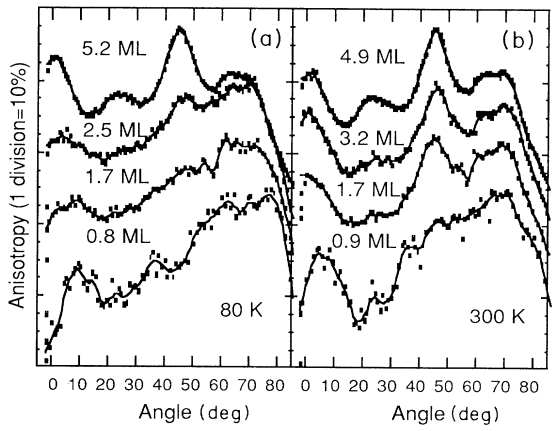

FIG. 27. XPS angular anisotropy for Co films grown on Cu(110) at (a) 80 K and (b) 300 K using Co $3p_{3/2}$ photoelectrons. Submonolayer anisotropies are somewhat unreliable (see text).

py is sharp and very similar to bulk Cu(110) [Fig. 1(b)]. Deposition of 0.9 ML at 300 K produces results similar to deposition at 80 K. Again the 1-ML film structure must be considered somewhat inconclusive based upon the XPS angular anisotropy alone. After deposition of 1.7 ML, consistent peaks develop in the angular anisotropy near 0° and 45°, which indicate the growth is not layer by layer. After deposition of 4.9 ML, the angular anisotropy peaks of the film sharpen only a little more. These data show that the phase of Co on Cu(110) is fcc (110) for films up to 5 ML thick, although the growth modes are very different for growth temperatures of 80 and 300 K.

LEED spots for a 1-ML Co film grown at 80 K are broad and form a $p(1\times1)$ pattern. After deposition of 2 ML and more, the LEED patterns are weak and broad steaks develop along $[1\bar{1}0]$. These streaks indicate disorder along the furrows of the surface and are expected for adatom diffusion along the furrows, which nucleates long, irregular clusters. After deposition of nearly 5 ML, the LEED pattern develops weak [001] streaks and the elongated spots collapse into two weak, symmetric spots, above and below the principal center spot along the [001] direction. This pattern indicates a regular ordering along the substrate furrows and persists for films up to at least 20 ML thick. Films grown at 300 K and less than 4 ML thick have LEED patterns that are $p(1\times1)$ with broad spots that oscillate with energy. Films about 4 ML thick have LEED patterns with weak $[1\bar{1}0]$ streaks. The streaks sharpen with increasing thickness, and there are indications of a (1×2) pattern for films 8 ML thick. Films that are 15 ML thick have a $c(2\times2)$ LEED pattern.

C. Discussion

The fraction of Cu in the exposed surface for both the Fe and Co films grown on Cu(110) are very similar. The 80-K grown films show Cu values very near the Cu(111) and Cu(100) percentages. Films grown at 300 K show a substantially larger fraction of Cu in the exposed surface when compared to films grown at 80 K or comparable films grown on Cu(111) and Cu(100). Qualitatively the results suggest considerable agglomeration and/or Cu surface segregation. The symmetric LEED patterns observed indicate that this process is not random but ordered with respect to the furrows in the (110) surface. 1- and 2-ML films show roughly 70% and 50% of the surface is Cu, respectively. Pure agglomeration suggests formation of 4-ML-thick clusters. The XPS angular anisotropies displayed in even the thinnest Co and Fe films imply a large fraction of the Co and Fe residing in the third or deeper layer. However, surface segregation is also likely on the grounds of surface free-energy differences and is consistent with the relatively slow decay of surface Cu (Figs. 24 and 26). Recent local-density-functional calculations[181] have suggested a related growth mode for Au/Ag(110): Au substitutes for the second Ag layer resulting in a Ag/Au/Ag sandwich structure. The growth process is driven by the heat of alloy formation for Au in Ag, which is exothermic. This intermixed growth mode has been largely confirmed by recent STM studies.[182] It is conceivable that a similar process could occur for Fe and/or Co on Cu(110), but minimization of the surface free energy could be the driving force.

XPS angular anisotropies shows both Fe and Co films are predominantly fcc(110) for thicknesses up to ~6 ML. The Co remains fcc up to at least 20 ML. Comparison of the forward-scattering anisotropies for Co and Fe films (Figs. 25 and 27, respectively) with the angular anisotropy for Cu(110) [Fig. 1(b)] show the Co films are ordered for both growth temperatures, while Fe films are better ordered for 300-K growth. Independent of the 80- or 300-K growth temperature, LEED patterns show streaks and splitting along the furrowed $[1\bar{1}0]$ direction. This structure is expected for diffusion along the furrows and occurs even at 80 K. Preliminary SPA-LEED data for Fe deposited on Cu(110) at 80 K support these observations.[102] Fe films grown at 80 K have XPS angular anisotropies that show deviations from ideal fcc(110) at a thickness of 5.1 ML, while the LEED shows growing disorder. Increasing the Fe growth temperature to 300 K improves the fcc(110) structure. An 8-ML Fe film grown at 300 K is no longer fcc(110) and has begun converting to a bcc phase. Electron microscopy measurements of electrodeposited films also showed a bcc component for films thicker than 30 Å.[179]

VI. CONCLUSIONS

The structure and morphology of Fe and Co films grown on Cu(100), Cu(110), and Cu(111) hold more similarities than differences. This can be understood in terms of the comparable Fe/Cu and Co/Cu system growth kinetics—despite profound changes in Fe, Co, and Cu mobilities with substrate growth temperature. Growth at low temperature (~80 K) is consistent with limited adatom mobility. Growth at moderate temperatures [~300 K for Cu(100) and Cu(111)] is distinguished by initial multilayer formation and is followed at higher temperatures [~400 K for Cu(100) and Cu(111)] by substantial Cu segregation. The growth temperature of the film affects the morphology of the film and can also affect the crystalline phase of the film. For example, Fe deposited on Cu(111) is predominantly bcc(110) for growth at 80 K but fcc(111) for growth at 300 K. Co deposited on Cu(111) is predominantly fcc(111), but for growth at 80 K there is a significant hcp(0001) component. In general, the quasiequilibrium Frank–van der Merwe, Volmer-Weber, and Stranski-Krastanov growth modes do not adequately describe the growth kinetics of the Fe/Cu and Co/Cu systems. Simple considerations of surface diffusion and surface free energies provide a basis for understanding the observed growth modes. It is reasonable to expect that other metastable metal-film/metal-substrate systems (for example, see Refs. 11 and 183–185) should also necessitate a more dynamic description than provided by the Frank–van der Merwe, Volmer-Weber and Stranski-Krastanov growth modes.

The particular conclusions of this investigation are the following.

(1) Forward scattering is a useful tool for examining surface relaxations as well as the crystalline structure of the film. A necessary complement to "surface techniques" such as LEED and forward scattering is an ele-

mental probe of only the top atomic layer. CO titration is such a technique.

(2) Growth at 80 K severely restricts thermally activated surface diffusion of Fe on Cu(100), (110), and (111) and Co on Cu(100) and (110). This low mobility results in 90% substrate coverage after deposition of ~3 ML. In comparison, the mobility Co on Cu(111) is higher, and 90% substrate coverage occurs after deposition of ~4 ML.

(3) Coverage of the Cu(100) substrate for growth at 80 K is slower than predicted by the downward funneling model[160,162,163] and nearer estimates for the Poisson model. However, this similarity does not necessarily imply that the film growth is genuinely random.

(4) The short-range order observed in LEED, the relatively slow substrate coverage, and the previous observation of RHEED oscillations indicate that Fe and Co atoms condensing on Cu(100) have enough mobility to cluster in small islands even at substrate growth temperatures where thermal diffusion is expected to be inoperative, 80 K.

(5) Growth at 300 K for Co and Fe films on Cu is *not* generally layer-by-layer FM growth. However, Fe and Co film growth on Cu(100) is roughly layer by layer between 2 and 10 ML.

(6) The initial growth mode at 300 K of Fe and Co on Cu(100) and Cu(111) is characterized by multilayer formation. Coverage of 90% of the substrate occurs for 4–6 ML of deposited material on Cu(100) and Cu(111). The initial growth mode at 300 K of Fe and Co on Cu(110) is complex and may include agglomeration and/or segregation. Growth on Cu(110) indicates a larger fraction of Cu in the exposed surface than for growth on (100) or (111) and 90% coverage is achieved for 7–8 ML of deposited material. In general, the fraction of Cu in the exposed surface appears to diminishes exponentially with the average thickness of the deposited material, but at different rates for the different substrates.

(7) Above 375 K for Cu(100) and 400 K for Cu(111), the initial growth of Co and Fe is accompanied by significant segregation (≤ 1 ML) of Cu to the surface of the film.

(8) Many of our results indicate that substrate steps play an important role in determining the morphology of the film. These results include the sensitivity of the CO-titration measurements to the Cu(100) substrate perfection and the measurement of 80% Cu in the exposed surface for 2.5 ML of Co deposited on a sputtered but unannealed Cu(111) substrate.

(9) The Fe film structure is initially lattice matched fcc. Transformation from fcc to bcc crystalline structures begins near 10 ML thicknesses on Cu(100) and Cu(110). The transformation occurs at a growth-temperature-dependent thickness on Cu(111), and for growth at 80 K the film is already bcc by completion of the first unit cell (3 ML). The fcc to bcc Fe transformation on Cu(100) and Cu(111) appears to be facilitated by the propagation of bulk misfit dislocations. The high-free-energy fcc(100) and fcc(110) surfaces display surface reconstructions.

(10) The Co film structure in initially latticed matched fcc with an hcp component on Cu(111) for growth at 80 K. Strong deviations from fcc occur after 8 ML thicknesses on Cu(100) and above 20 ML thicknesses on Cu(110). Interlayer relaxations are observed for films on Cu(100) and reconstructions occurs on Cu(110).

(11) In separate studies to be published elsewhere, we examine the perpendicular magnetic anisotropies in these systems.[184] In general, perpendicular anisotropies in the Fe film were found to be enhanced by low-temperature growth. Perpendicular remanent magnetizations with square hysteresis loops were observed for films thicknesses up to 7 ML of fcc Fe/Cu(100), 6 ML of fcc Fe/Cu(110), and 4.5 ML of bcc Fe/Cu(111). Co films had a perpendicular remanence only when grown on Cu(111) at 80 K and annealed to 300 K, for films up to 5 ML thick.

(12) The structures and morphologies of these systems are complex because the growth modes are complex. Inadequate structural characterization yields (seemingly) contradictory conclusions from one group to another. Furthermore, the subleties of the structural relaxations in the films, the metastable crystalline phases of the films and the magnetic properties of the films cannot be expected to be reproduced or adequately understood through the theories of simple or idealized models of growth that the data show to be unrealistic.

ACKNOWLEDGMENT

The authors wish to acknowledge the excellent technical support of F. Kovanic.

[1]L. M. Falicov, D. T. Pierce, S. D. Bader, R. Gronsky, K. B. Hathaway, H. J. Hopster, D. N. Lambeth, S. S. P. Parkin, G. Prinz, M. Salamon, I. K. Schuller, and R. H. Victora, J. Mater. Res. **5**, 1299 (1990).

[2]E. Bauer, Appl. Surf. Sci. **11/12**, 479 (1982).

[3]L. Z. Mezey and J. Giber, Jpn. J. Appl. Phys. **21**, 1569 (1982).

[4]A. R. Miedema, Z. Metallkde. **69**, 455 (1978).

[5]U. Gradmann, W. Kümmerle, and P. Tillmanns, Thin Solid Films **34**, 249 (1976).

[6]W. Kümmerle and U. Gradmann, Solid State Commun. **24**, 33 (1977).

[7]W. Kümmerle and U. Gradmann, Phys. Status Solidi A **45**, 171 (1978).

[8]C. Rau, C. Schneider, G. Xing, and K. Jamison, Phys. Rev. Lett. **57**, 3221 (1986).

[9]Y. Darici, J. Marcano, H. Min, and P. A. Montano, Surf. Sci. **195**, 566 (1988).

[10]D. Tian, F. Jona, and P. M. Marcus, Phys. Rev. B **45**, 11 216 (1992).

[11]M. F. Onellion, C. L. Fu, M. A. Thompson, J. L. Erskine, and A. J. Freeman, Phys. Rev. B **33**, 7322 (1986).

[12]Y. C. Lee, H. Min, and P. A. Montano, Surf. Sci. **166**, 391 (1986).

[13]M. Onellion, M. A. Thompson, J. L. Erskine, B. Duke, and A. Paton, Surf. Sci. **179**, 219 (1987).

[14]D. Pescia, M. Stampanoni, G. L. Bona, A. Vaterlaus, R. F. Willis, and F. Meier, Phys. Rev. Lett. **58**, 2126 (1987).

[15]M. Stampononi, A. Vaterlaus, M. Aeschlimann, F. Meier, and

D. Pescia, J. Appl. Phys. **64**, 5321 (1988).
[16]W. Daum, C. Stuhlmann, and H. Ibach, Phys. Rev. Lett. **60**, 2741 (1988).
[17]Y. Darici, J. Marcano, H. Min, and P. A. Montano, Surf. Sci. **217**, 521 (1989).
[18]L. Gonzalez, R. Miranda, M. Salmerón, J. A. Vergés, and F. Ynduráin, Phys. Rev. B **24**, 3245 (1981).
[19]R. Miranda, D. Chandesris, and J. Lecante, Surf. Sci. **130**, 269 (1983).
[20]A. Clarke, G. Jennings, R. F. Willis, P. J. Rous, and J. B. Pendry, Surf. Sci. **187**, 327 (1987).
[21]J. J. de Miguel, A. Cebollada, J. M. Gallego, S. Ferrer, R. Miranda, S. C. M. P. Bressler, J. Garbe, K. Bethke, and J. Kirshner, Surf. Sci. **211/212**, 732 (1989).
[22]C. M. Schneider, P. Bressler, P. Schuster, J. Kirschner, J. J. de Miguel, and R. Miranda, Phys. Rev. Lett. **64**, 1059 (1990).
[23]D. Kerkmann, D. Pescia, J. W. Krewer, and E. Vescovo, Z. Phys. B **85**, 311 (1991).
[24]R. Germar, W. Dürr, J. W. Krewer, D. Pecsia, and W. Gudat, Appl. Phys. A **47**, 393 (1988).
[25]J. R. Chelikowsky, Surf. Sci. **139**, L197 (1984).
[26]S. Mukherjee and J. L. Morán-López, Surf. Sci. **188**, L742 (1987).
[27]P. M. Ossi, Surf. Sci. **201**, L519 (1988).
[28]T. T. Tsong and P. L. Cowan, Crit. Rev. Solid State Mater. Sci. **7**, 289 (1978).
[29]G. Ehrlich, in *Phase Transitions in Condensed Systems,* edited by G. S. Cargill III, F. Spaepen, and K.-N. Tu, MRS Symposia Proceedings No. 57 (Materials Research Society, Pittsburgh, 1987), p. 313.
[30]S. C. Wang and G. Ehrlich, Phys. Rev. **62**, 2297 (1989).
[31]C. Chen and T. T. Tsong, Phys. Rev. Lett. **64**, 3147 (1990).
[32]G. L. Kellogg and P. J. Feibelman, Phys. Rev. Lett. **64**, 3143 (1990).
[33]S. C. Wang and G. Ehrlich, Phys. Rev. Lett. **67**, 2509 (1991).
[34]P. Wynblatt, Phys. Status Solidi **36**, 797 (1969).
[35]H. P. Bonzel, CRC Crit. Rev. Solid State Sci. **6**, 171 (1976).
[36]H. P. Bonzel and E. E. Latta, Surf. Sci. **76**, 275 (1978).
[37]R. Butz and H. Wagner, Surf. Sci. **87**, 69 (1979).
[38]H. P. Hölzl, G. Porsch, and P. Schrammen, Surf. Sci. **97**, 529 (1980).
[39]P. Schrammen and J. Hölzl, Surf. Sci. **130**, 203 (1983).
[40]H. P. Bonzel, in *Surface Mobilities on Solids Materials,* edited by V. T. Binh (Plenum, New York, 1983), p. 195.
[41]D. Stark, Surf. Sci. **189/190**, 1111 (1987).
[42]G. L. Kellogg, Surf. Sci. **187**, 153 (1987).
[43]P. R. Schwoebel and G. L. Kellogg, Phys. Rev. B **38**, 5326 (1988); Phys. Lett. **61**, 578 (1988).
[44]T.-S. Lin and Y.-W. Chung, Superlatt. Microstruct. **6**, 709 (1988).
[45]J. P. Bourdin, J. P. Ganachaud, J. P. Jardin, D. Spanjaard, and M. C. Desjonquéres, J. Phys. F **18**, 1801 (1988).
[46]J. W. M. Frenken, J. P. Toennies, and C. Wöll, Phys. Rev. Lett. **60**, 1727 (1988).
[47]R. Gomer, Rep. Prog. Phys. **53**, 917 (1990).
[48]J. D. Wrigley and G. Ehrlich, Phys. Rev. Lett. **44**, 661 (1980).
[49]H.-J. Ernst, F. Fabre, and J. Lapujoulade, Phys. Rev. B **46**, 1929 (1992).
[50]M. Breeman and D. O. Boerma, Phys. Rev. B **46**, 1703 (1992).
[51]J. J. de Miguel, A. Cebollada, J. M. Gallego, J. Ferron, and S. Ferrer, J. Cryst. Growth **88**, 442 (1988).
[52]L. Hansen, P. Stoltze, K. W. Jacobsen, and J. K. Nørskov, Phys. Rev. B **44**, 6523 (1991).
[53]It is interesting to note that these calculations indicate that exchange-mediated diffusion is preferable on Cu(100), and exchange diffusion is only about 0.1 eV larger than diffusion over the long bridge path on Cu(110). This is comparable to field-ion-microscope experiments that have shown that exchange-mediated diffusion is the lowest energy path of Ir on Ir(100) (Ref. 31) and Ir(110) (Ref. 48).
[54]A. R. Miedema and J. W. F. Dorleijn, Surf. Sci. **95**, 447 (1980).
[55]The Cu(100) experimental activation energies (0.28, 0.39, and 0.48 eV) actually agree better with the predicted activation energy [from Hansen *et al.* (Ref. 52)] for bridge path diffusion ($\sim$0.4 eV) than exchange diffusion (0.18 eV), but this similarity may be fortuitous. Alternatively, Hansen *et al.* show an $\sim$0.9-eV decrease in barrier energy by including a one-electron correction. It is conceivable that a small change to this one-electron correction (e.g., due to a reduced electronic bandwidth) could significantly improve the agreement with experiment. Such a modification should not alter the calculated value for Cu(111), but could change the calculated value for a relaxed Cu(110) surface.
[56]W. F. Egelhoff, Jr., J. Vac. Sci. Technol. A **7**, 2060 (1989).
[57]S. A. Chambers, T. J. Wagener, and J. H. Weaver, Phys. Rev. B **36**, 8992 (1987).
[58]G. J. Mankey, M. T. Kief, and R. F. Willis, J. Vac. Sci. Technol. A **9**, 1595 (1991); G. J. Mankey, M. T. Kief, F. Huang, and R. F. Willis (unpublished).
[59]D. A. Steigerwald and W. F. Egelhoff, Jr., Surf. Sci. **192**, L887 (1987).
[60]M. H. Yang and C. P. Flynn, Phys. Rev. Lett. **62**, 2476 (1989).
[61]C. P. Flynn, J. Phys. F **18**, L195 (1988).
[62]D. A. Steigerwald, I. Jacob, and W. F. Egelhoff, Jr., Surf. Sci. **202**, 472 (1988).
[63]J. S. Ahearn, Jr., J. P. Monaghan, Jr., and J. W. Mitchell, Rev. Sci. Instrum. **41**, 1853 (1970).
[64]F. W. Young, Jr., and T. R. Wilson, Rev. Sci. Instrum. **32**, 559 (1961).
[65]W. F. Egelhoff, Jr., J. Vac. Sci. Technol. A **7**, 3123 (1989).
[66]H. Glatzel, T. Fauster, B. M. U. Scherzer, and V. Dose, Surf. Sci. **254**, 58 (1991).
[67]H. Landskron, G. Schmidt, K. Heinz, K. Müller, C. Stulmann, U. Beckers, M. Wuttig, and H. Ibach, Surf. Sci. **256**, 115 (1991).
[68]C. S. Fadley, Phys. Scr. **T17**, 39 (1987).
[69]S. A. Chambers, Adv. Phys. **40**, 357 (1991).
[70]H. Li and B. P. Tonner, Phys. Rev. B **40**, 10241 (1989); Surf. Sci. **237**, 141 (1990).
[71]A. K. Schmid and J. Kirschner, Ultramicroscopy **42-44**, 483 (1992).
[72]W. F. Egelhoff, Jr., Crit. Rev. Solid State Mater. Sci. **16**, 213 (1990).
[73]E. L. Bullock and C. S. Fadley, Phys. Rev. B **31**, 1212 (1985).
[74]W. A. Jesser and J. W. Matthews, Philos. Mag. **15**, 1097 (1967).
[75]W. A. Jesser and J. W. Matthews, Philos. Mag. **17**, 595 (1968).
[76]H. J. G. Draaisma, H. M. van Noort, and F. J. A. den Broeder, Thin Solid Films **126**, 117 (1985).
[77]M. Kato, S. Fukase, A. Sato, and T. Mori, Acta. Metall. **34**, 1179 (1986).
[78]Y. Ando and D. J. Dingley, Jpn. J. Appl. Phys. **29**, 939 (1990).
[79]M. Wada, S. Uda, and M. Kato, Philos. Mag. A **59**, 31 (1989).
[80]U. Gradmann and P. Tillmanns, Phys. Status Solidi A **44**, 539 (1977).
[81]F. Pontkees and H. Nedermeyer, Physica B **161**, 276 (1989).
[82]U. Gradmann and H. O. Isbert, J. Magn. Magn. Mater. **15-18**, 1109 (1980).

[83]C. H. Lee, H. He, F. J. Lamelas, W. Vavra, C. Uher, and R. Clarke, Phys. Rev. B **42**, 1066 (1990).
[84]K. Le Dang, P. Veillet, H. He, F. J. Lamelas, C. H. Lee, and R. Clarke, Phys. Rev. B **41**, 12 902 (1990).
[85]H. A. M. de Gronckel, K. Kopinga, W. J. M. de Jonge, P. Panissod, J. P. Schillé, and F. J. A. den Broeder, Phys. Rev. B **44**, 9100 (1991).
[86]H. A. M. de Gronckel, J. A. M. Bienert, F. J. A. den Broeder, and W. J. M. de Jonge, J. Magn. Magn. Mater. **93**, 457 (1991).
[87]C. Mény, P. Panissod, and R. Loloee, Phys. Rev. B **45**, 12 269 (1992).
[88]D. Chandesris, P. Roubin, and G. Rossi, Topics, Cur. Chem. **147**, (1988).
[89]P. Roubin, D. Chandesris, G. Rossi, and J. Lecante, J. Phys. F **18**, 1165 (1988).
[90]F. J. Lamelas, C. H. Lee, H. He, W. Vavra, and R. Clarke, Phys. Rev. B **40**, 5837 (1989).
[91]C. M. Wei, T. C. Zhao, and S. Y. Tong, Phys. Rev. Lett. **65**, 2278 (1990).
[92]U. Gradmann and J. Muller, Z. Angew. Phys. **30**, 87 (1970).
[93]R. Miranda, F. Yndurain, D. Chandesris, J. Lecante, and Y. Petroff, Phys. Rev. B **25**, 527 (1982).
[94]Q. Chen, Ph.D. thesis, University of Wisconsin–Madison, 1991.
[95]Q. Chen, M. Onellion, and A. Wall (unpublished).
[96]J. Kohlhepp, H. J. Elmers, S. Cordes, and U. Gradmann, Phys. Rev. B **45**, 12 287 (1992).
[97]R. Ramirez, A. Rahman, and I. K. Schuller, Phys. Rev. B **30**, 6208 (1984).
[98]E. Bauer and J. H. van der Merwe, Phys. Rev. B **33**, 3657 (1986).
[99]A. Brodde and H. Neddermeyer, Ultramicroscopy **42-44**, 556 (1992).
[100]B. Poelsema, R. Kunkel, N. Nagel, A. F. Becker, G. Rosenfeld, L. K. Verheij, and G. Comsa, Appl. Phys. A **53**, 369 (1991).
[101]R. Kunkel, B. Poelsema, L. Verheij, and G. Comsa, Phys. Rev. Lett. **65**, 733 (1990).
[102]G. L. Nyberg, M. T. Kief, and W. F. Egelhoff, Jr. (unpublished).
[103]D. Tian, H. Li, F. Jona, and P. M. Marcus, Solid State Commun. **80**, 783 (1991).
[104]S. Andrieu, M. Piecuch, and J. F. Bobo, Phys. Rev. B **46**, 4909 (1992).
[105]G. H. Olsen and W. A. Jesser, Acta Metall. **19**, 1299 (1971).
[106]K. E. Easterling and H. M. Miekk-oja, Acta Metall. **15**, 1133 (1967).
[107]S. Tanuma, C. J. Powell, and D. R. Penn, Surf. Inter. Anal. **17**, 911 (1991).
[108]C. M. Wei, T. C. Zhao, and S. Y. Tong, Phys. Rev. Lett. **65**, 2278 (1990).
[109]C. M. Wei, T. C. Zhao, and S. Y. Tong, Phys. Rev. B **43**, 6354 (1991).
[110]T. Nishizawa and K. Ishida, Bull. Alloy Phase Diagrams **5**, 161 (1984).
[111]T. Nishizawa and K. Ishida, Bull. Alloy Phase Diagrams **4**, 387 (1983).
[112]D. E. Sanders and A. E. DePristo, Surf. Sci. **260**, 116 (1992).
[113]Note that these calculations (Ref. 112) fail to permit the potentially lower energy path of coordinated exchange, but this mechanism is not expected to be important for (111) fcc metal surfaces (Ref. 52).
[114]TEM studies of sputtered Fe/Cu(111) multilayers indicate a slightly thicker transitional range for room-temperature grown films as between 6 and 12 Å (Ref. 76). This small change in thickness is not unexpected due to the different growth dynamics for sputtered films.
[115]S. C. Wang and G. Ehrlich, in *The Structure of Surfaces III,* edited by S. Y. Tong, M. A. Van Hove, K. Takayanagi, and X. D. Xie (Springer-Verlag, Berlin, 1991), p. 317.
[116]Wang and Ehrlich (Ref. 33) distinguish two types of steps at the cluster edge, which they refer to as *A* and *B*. They report different kinetics for atom incorporation into descending steps of either type *A* or type *B*. The step-type dependence can be related to the different stacking of the step edge adatoms: an atom at the edge of a type-*A* (*B*) step is in a hcp (fcc) stacking site. It follows that incorporation into ascending steps will also vary with step type. In the case of Co, the hcp incorporation at an *A* step could be favored; this would preferentially nucleate hcp double layers.
[117]Note that de Gronckel *et al.* (Ref. 85) suggest that the structure of the Co/Cu interface is equivalent to the Cu/Co interface. However, free-energy differences argue against this symmetry. Instead the Co/Cu interface may be a mixed 2 ML and the Cu/Co interface would be more abrupt.
[118]C. Liu, E. R. Moog, and S. D. Bader, Phys. Rev. Lett. **60**, 2422 (1988).
[119]W. F. Egelhoff, Jr. and M. T. Kief, Phys. Rev. B **45**, 7795 (1992).
[120]O. Haase, Z. Naturforsch. A **14**, 920 (1959).
[121]D. C. Hothersall, Philos. Mag. **13**, 1023 (1967).
[122]G. H. Olsen and W. A. Jesser, Acta Metall. **19**, 1009 (1971).
[123]A. A. Hezaevh, G. Jennings, D. Pescia, R. F. Willis, K. Prince, M. Surman, and A. Bradshaw, Solid State Commun. **57**, 329 (1986).
[124]A. Clarke, P. J. Rous, M. Arnott, G. Jennings, and R. F. Willis, Surf. Sci. **192**, L843 (1987).
[125]C. Egawa, E. M. McCash, and R. F. Willis, Surf. Sci. **215**, L271 (1989).
[126]F. Jona and P. M. Marcus, Surf. Sci. **223**, L897 (1989).
[127]S. H. Lu, J. Quinn, D. Tian, F. Jona, and P. M. Marcus, Surf. Sci. **209**, 364 (1989).
[128]J. Thomassen, B. Feldmann, and M. Wuttig, Surf. Sci. **264**, 406 (1992); J. Thomassen, F. May, B. Feldman, M. Wuttig, and H. Ibach, Phys. Rev. Lett. **69**, 3831 (1992).
[129]H. Magnan, D. Chandesris, B. Villette, O. Heckmann, and J. Lecante, Phys. Rev. Lett. **67**, 859 (1991).
[130]P. Xhonneux and E. Courtens, Phys. Rev. B **46**, 556 (1992).
[131]D. D. Chambliss, R. J. Wilson, and S. Chiang, J. Vac. Sci. Technol. A **10**, 1993 (1992).
[132]P. Dastoor, M. Arnott, E. M. McCash, and W. Allison, Surf. Sci. **272**, 154 (1992).
[133]A. Brodde and H. Neddermeyer (unpublished).
[134]W. Becker, H.-D. Pfannes, and W. Keune, J. Magn. Magn. Mater. **35**, 53 (1983).
[135]W. Keune, R. Halbauer, U. Gonser, J. Lauer, and D. L. Williamson, J. Appl. Phys. **48**, 2976 (1977); W. A. A. Macedo and W. Keune, Phys. Rev. Lett. **61**, 475 (1988); W. A. A. Macedo, W. Keune, and E. D. Ellerbrock, J. Magn. Magn. Mater. **93**, 552 (1991).
[136]S. D. Bader and E. R. Moog, J. Appl. Phys. **61**, 3729 (1987).
[137]J. A. C. Bland, D. Pescia, and R. F. Willis, Phys. Rev. Lett. **58**, 1244 (1987).
[138]P. A. Montano, G. W. Fernando, B. R. Cooper, E. R. Moog, H. M. Naik, S. D. Bader, Y. C. Lee, Y. N. Darici, H. Min, and J. Marcano, Phys. Rev. Lett. **59**, 1041 (1987).
[139]T. Beier, D. Pescia, M. Stampanoni, A. Vaterlaus, and F. Meier, Appl. Phys. A **47**, 73 (1988).

[140]W. Schwarzacher, W. Allison, R. F. Willis, J. Penfold, R. C. Ward, I. Jacob, and W. F. Egelhoff, Jr., Solid State Commun. **71**, 563 (1989).
[141]F. J. Himpsel, Phys. Rev. Lett. **67**, 2363 (1991).
[142]M. Doyama, M. Matsui, H. Matsuoka, S. Mitani, and K. Doi, J. Magn. Magn. Mater. **93**, 374 (1991).
[143]C. Liu, E. R. Moog, and S. D. Bader, J. Appl. Phys. **64**, 5325 (1988).
[144]J. F. Cochran, J. M. Rudd, M. From, B. Heinrich, W. Bennett, W. Schwarzacher, and W. F. Egelhoff, Jr., Phys. Rev. B **45**, 4676 (1992).
[145]D. P. Pappas, K.-P. Kämper, and H. Hopster, Phys. Rev. Lett. **64**, 3179 (1990); D. P. Pappas, C. R. Brundle, and H. Hopster, Phys. Rev. B **45**, 8169 (1992).
[146]R. Allenspach and A. Bischof, Phys. Rev. Lett. **69**, 3385 (1992).
[147]W. A. Jesser and J. W. Matthews, Philos. Mag. **17**, 461 (1968).
[148]M. T. Kief, G. J. Mankey, and R. F. Willis, in *The Structure of Surfaces III* (Ref. 115), p. 422.
[149]S. Ferrer, E. Vlieg, and I. K. Robinson, Surf. Sci. **250**, L363 (1991).
[150]T. Beier, H. Jahrreiss, D. Pescia, T. Woike, and W. Gudat, Phys. Rev. Lett. **61**, 1875 (1988).
[151]D. Pescia, R. F. Willis, and J. A. C. Bland, Surf. Sci. **189/190**, 724 (1987).
[152]D. Kerkmann, Appl. Phys. A **49**, 523 (1989).
[153]H. P. Oepen, M. Benning, H. Ibach, C. M. Schneider, and J. Kirschner, J. Magn. Magn. Mater. **86**, L137 (1990).
[154]J. J. de Miguel, A. Cebollada, J. M. Gallego, and R. Miranda, in *Kinetics of Ordering and Growth at Surfaces,* edited by M. G. Lagally (Plenum, New York, 1990), p. 483.
[155]J. J. de Miguel, A. Cebollada, J. M. Gallego, R. Miranda, C. M. Schneider, P. Schuster, and J. Kirschner, J. Magn. Magn. Mater. **93**, 1 (1991).
[156]M. T. Kief, G. J. Mankey, and R. F. Willis, J. Appl. Phys. **69**, 5000 (1991); M. T. Kief, Ph.D. thesis, The Pennsylvania State University, University Park, 1991.
[157]P. Krams, F. Lauks, R. L. Stamps, B. Hillebrands, and G. Güntherodt, Phys. Rev. Lett. **69**, 3674 (1992).
[158]K.-P. Kämper, D. L. Abraham, and H. Hopster, Phys. Rev. B **45**, 14 335 (1992).
[159]C. Kittel and H. Kroemer, *Thermal Physics* (Freeman, San Francisco, 1980).
[160]J. W. Evans, Phys. Rev. B **39**, 5655 (1989).
[161]W. F. Egelhoff, Jr. and I. Jacob, Phys. Rev. Lett. **62**, 921 (1989).
[162]J. W. Evans, D. E. Sanders, P. A. Thiel, and A. E. DePristo, Phys. Rev. B **41**, 5410 (1990).
[163]P. J. Schmitz, W.-Y. Leung, G. W. Graham, and P. A. Thiel, Phys. Rev. B **40**, 11 477 (1989).
[164]D. E. Sanders and J. W. Evans, in *The Structure of Surfaces III* (Ref. 115), p. 38.
[165]W. F. Egelhoff, Jr., Phys. Rev. B **30**, 1052 (1984).
[166]Note that an alternate approach has been presented that compares the forward-scattering enhancement to ideal layer-by-layer growth (Ref. 70). Our approach is specialized to interpreting initial agglomeration.
[167]S. T. Purcell, A. S. Arrott, and B. Heinrich, J. Vac. Sci. Technol. B **6**, 794 (1988).
[168]K. D. Gronwald and M. Henzler, Surf. Sci. **117**, 180 (1982).
[169]M. A. Van Hove, W. H. Weinberg, and C. Chan, *Low-Energy Electron Diffraction* (Springer-Verlag, Berlin, 1986).
[170]D. P. Pappas, Ph.D. thesis, University of California, Irvine, 1990.
[171]M. A. Van Hove, R. J. Koestner, P. C. Stair, J. P. Bibérian, L. L. Kesmodel, I. Bartos, and G. A. Somorjai, Surf. Sci. **103**, 189 (1981).
[172]M. T. Kief and W. F. Egelhoff, Jr. (unpublished).
[173]J. L. Murray, L. H. Bennett, and H. Baker, in *Binary Alloy Phase Diagrams,* edited by T. Massalski (American Society for Metals, Metals Park, Ohio, 1986).
[174]C. M. Schneider, J. J. de Miguel, P. Schuster, R. Miranda, B. Heinrich, and J. Kirshner, in *Science and Technology of Nanostructured Magnetic Materials,* edited by G. C. Hadjipanayis and G. A. Prinz (Plenum, New York, 1991), p. 37.
[175]F. Falo, I. Cano, and M. Salermón, Surf. Sci. **143**, 303 (1984).
[176]R. D. Young and D. C. Schubert, J. Chem. Phys. **42**, 3943 (1965).
[177]Strictly speaking the Monte Carlo simulations of Young and Schubert address growth of bcc W(100). We believe it is reasonable to expect that a similar coverage dependence on hopping can be expected for the first few layers of fcc (100) Fe or Co. Also high adatom mobility would increase the fraction of Cu at the surface, as occurs at 300 K, but agglomeration at 80 K seems less likely.
[178]F. J. Himpsel, Phys. Rev. B **44**, 5966 (1991).
[179]J. G. Wright, Philos. Mag. **24**, 217 (1971).
[180]J. Marcano, Y. Darici, H. Min, Y. Yin, and P. A. Montano, Surf. Sci. **217**, 1 (1989).
[181]C. T. Chan, K. P. Bohnen, and K. M. Ho, Phys. Rev. Lett. **69**, 1672 (1992).
[182]S. Rousset, S. Chiang, D. E. Fowler, and D. D. Chambliss, Phys. Rev. Lett. **69**, 3200 (1992).
[183]J. P. Biberian and G. A. Somorjai, J. Vac. Sci. Technol. **16**, 2073 (1979).
[184]S. D. Bader, Proc. IEEE **78**, 909 (1990).
[185]G. A. Prinz, J. Magn. Magn. Mater. **100**, 469 (1991).
[186]M. T. Kief and W. F. Egelhoff, Jr., in *Proceedings of MMM-92* [J. Appl. Phys. (to be published)].